CDDpress

www.nature.com/cdd

ARTICLE

Check for updates

# Wun2-mediated integrin recycling promotes apoptotic cell clearance in *Drosophila melanogaster*

Ning Gao[1,2,3], Qian Zheng[1,3], Yanzhe Wang[1,3], Xiaowen Li[1], Zhi Li[1] and Hui Xiao[1]✉



Apoptotic cell (AC) clearance is a complex process in which phagocytes recognize, engulf, and digest ACs during organismal development and tissue homeostasis. Impaired efferocytosis results in developmental defects and autoimmune diseases. In the current study, we performed RNA-sequencing to systematically identify regulators involved in the phagocytosis of ACs by *Drosophila melanogaster* macrophage-like S2 cells, followed by targeted RNA interference screening. Wunen2 (Wun2), a homolog of mammalian lipid phosphate phosphatase (LPP), was deemed as required for efferocytosis both in vitro and in vivo. However, efferocytosis was independent of Wun2 phosphatase activity. Proteomic analysis further revealed that Rab11 and its effector Rip11 are interaction partners of Wun2. Therefore, Wun2 collaborates with Rip11 and Rab11 to mediate efficient recycling of the phagocytic receptor βv integrin subunit to the plasma membrane. The loss of Wun2 results in the routing of βv integrin subunit (Itgbn) into lysosomes, leading to its degradation. The deficiency of βv integrin subunit on the cell surface leads to aberrant and disorganized actin cytoskeleton, thereby influencing the formation of macrophage pseudopodia toward ACs and thus failure to engulf them. The findings of this study provide insights that clarify how phagocytes coordinate AC signals and adopt a precise mechanism for the maintenance of engulfment receptors at their cell membrane surface to regulate efferocytosis.

*Cell Death & Differentiation* (2022) 29:2545–2561; https://doi.org/10.1038/s41418-022-01039-3

## INTRODUCTION

Apoptosis is a crucial type of programmed cell death controlled and executed via an evolutionarily conserved pathway. At the final stage of apoptosis, cells are swiftly removed by phagocytes [1, 2]. The clearance of dead cells, termed 'efferocytosis,' is critical for homeostasis, and failure to properly clear ACs is linked to developmental abnormalities, neurodegenerative diseases, chronic inflammation, and autoimmune diseases [3–6].

Over the past decades, the use of *Drosophila* species in genetics has continually provided information on vertebrates, facilitating the development of important therapeutic targets for defective cell clearance in organisms [7]. Several key proteins required for ACs clearance have been identified in *D. melanogaster*; for example, Draper (Drpr) [8, 9], Croquemort (Crq) [10, 11], and αPS3/βv integrin [12, 13]. However, the detailed molecular mechanisms and signals associated with efferocytosis have not been elucidated.

*Wunen* (*wun*) and *Wunen2* (*wun2*) encode the *D. melanogaster* homologs of lipid phosphate phosphatases 1, 2, and 3, all comprising six transmembrane α-helices with the C- and N-termini facing the cytoplasmic side and the catalytic site facing the outside of cells or the luminal side of organellar membranes [14]. LPPs can dephosphorylate several phosphate esters, including sphingosine-1-phosphate (S1P), ceramide-1-phosphate (C1P), phosphatidic acid (PA), and lysophosphatidic acid (LPA) [15, 16]. Although Wun and Wun2 have redundant functions in somatic cells to direct primordial germ cells or pole cell migration and survival [15, 17, 18], their localization and function in the trachea are distinct [19]. Low expression of LPP3 in triple-negative breast cancer can hinder the recruitment of immune cells, resulting in the blockage of cancer cell clearance [20]. However, studies on LPPs in immunology are limited, and the possible association of LPPs with efferocytosis remains poorly understood.

Integrins are conserved transmembrane receptors consisting of α and β heterodimers [21]. These proteins connect the extracellular matrix to the cytoskeleton, allowing phagocytic cells to adjust membrane protrusions according to the shape and size of the ACs or microorganisms to be engulfed [22]. The integrin αPS3/βv heterodimer is involved in the phagocytosis of ACs and *Staphylococcus aureus* in *D. melanogaster* phagocytes [13]. During phagocytosis, cell surface integrins are endocytosed and undergo endosomal sorting, a process in which Rab family proteins and their effectors are involved [23–26]. Although the mechanisms for integrin recycling are well-established, those underlying its degradation are not well understood.

In the present study, we screened *D. melanogaster* macrophage-like lineage S2 cells for novel gene candidates required for the phagocytosis of ACs using whole transcriptome analysis (RNA-sequencing). The LPP Wun2 was identified, and the non-phosphatase domain of Wun2 could interact with the Rab11 effector Rip11 C2 domain and βv integrin. This interaction prevented the lysosomal degradation and transport of βv integrin

[1]College of Life Sciences, Shaanxi Normal University, Xi'an 710119 Shaanxi, China. [2]Medical College of Yan'an University, Yan'an, Shaanxi 716000, China. [3]These authors contributed equally: Ning Gao, Qian Zheng, Yanzhe Wang ✉email: huixiao@snnu.edu.cn

Edited by E. Baehrecke

Received: 31 August 2021 Revised: 25 June 2022 Accepted: 4 July 2022
Published online: 15 July 2022

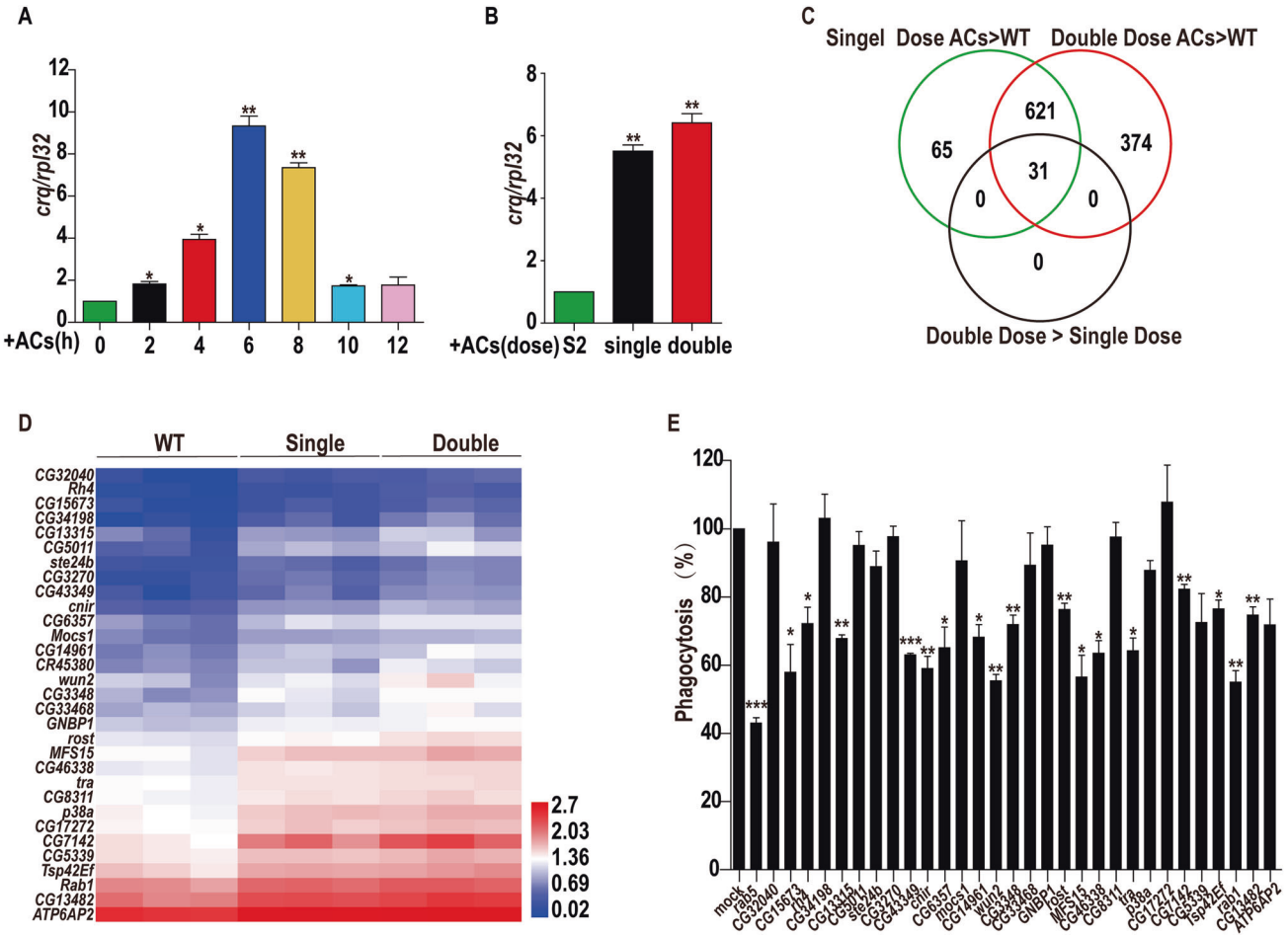


**Fig. 1 RNA-sequencing and RNAi screening of candidate genes involved in efferocytosis. A** *crq* mRNA levels were quantified at different ACs incubation times in S2 cells by quantitative real-time PCR (qRT-PCR) and normalized to *rpl32* mRNA. The data were collected from three independent experiments; 0 h samples were used as the control. The asterisks above the column denote a significantly higher gene expression than that detected at 0 h. Data are presented as mean ± SEM, (ANOVA; $*p < 0.05$; $**p < 0.01$). **B** qRT-PCR analysis of *crq* mRNA levels in S2 cells incubated with a single or double dose of ACs and normalized to *rpl32* mRNA (ANOVA; $**p < 0.01$; $n = 3$ replicates). **C** Venn diagram showing the number of upregulated genes in S2 cells identified by RNA-sequencing after incubation with single or double doses of ACs for 6 h. A total of 717 genes were upregulated in a single dose of ACs (green), and 1026 genes were upregulated after incubation with double doses of ACs (red). A total of 652 genes were upregulated in both treatments, and the upregulation levels of 31 genes were 1.5-fold greater in the double dose compared to the single dose (black). Three repetitions were performed for each group. **D** Heatmap representing the 31 transcripts that were upregulated in a dose-dependent manner, with FPKM 1.5-fold greater in the double dose than in the single dose. Each column represents an independent sample. The color key and density plots represent the levels of regulation. **E** Phagocytosis ratio of ACs in S2 cells treated with dsRNA. Three independent experiments were repeated. Bars represent mean phagocytosis percentage ± SEM (ANOVA; $*p < 0.05$; $**p < 0.01$; $***p < 0.001$).

from Rab11 recycling endosomes to the plasma membrane to promote ACs clearance. Our study reveals the critical role of Wun2 in the Rab11 recycling pathway to prevent βv integrin degradation and identifies the important function of Wun2 in efferocytosis, along with implications for the treatment of diseases that result from impaired efferocytosis.

## RESULTS

### Screening of candidate genes required for efferocytosis in *D. melanogaster* macrophages

*Crq* is defined as an engulfment receptor; its expression can be regulated by the extent of cell apoptosis [11]. During the process of ACs clearance in S2 cells, the expression of *crq* was time-dependent (Fig. 1A) and dose-dependent (Fig. 1B). Therefore, we performed transcriptomic analysis of the S2 cells engulfing a single or double dose of ACs for 6 h; 652 genes were upregulated in a dose-dependent manner (Fig. 1C). Thirty-one of these genes yielded fragments per kilobase of transcript per million mapped reads (FPKM) values in the double dose incubation that were 1.5-fold higher than those in the single dose incubation (Fig. 1D and Supplementary Table 1). Individually silencing 17 of these genes resulted in an obvious reduction of efferocytosis efficiency in S2 cells (Fig. 1E); *wun2* RNA interference (RNAi) cells exhibited the lowest phagocytosis rate; therefore, *wun2* was selected for further analysis.

### *wun2* is required for efferocytosis in S2 cells and *D. melanogaster* macrophages

In S2 cells, ACs incubation elevated the transcriptional level of *wun2* for 8 h (Fig. 2A). However, *wun2* RNAi led to a significant decrease in the phagocytosis ratio (Fig. 2B, C and Supplementary Fig. 1A). For the in vivo assays, we generated an eight-base pair-deleted $wun2^{KO}$ mutant fly via CRISPR/Cas9; this frameshift mutation led to the early termination of Wun2 translation (Fig. 2D and Supplementary Fig. 2A), and both PCR and immunofluorescence staining confirmed $wun2^{KO}$ as a null allele mutant (Supplementary Fig. 2B–D). The stage 13 $wun2^{KO}$ embryo

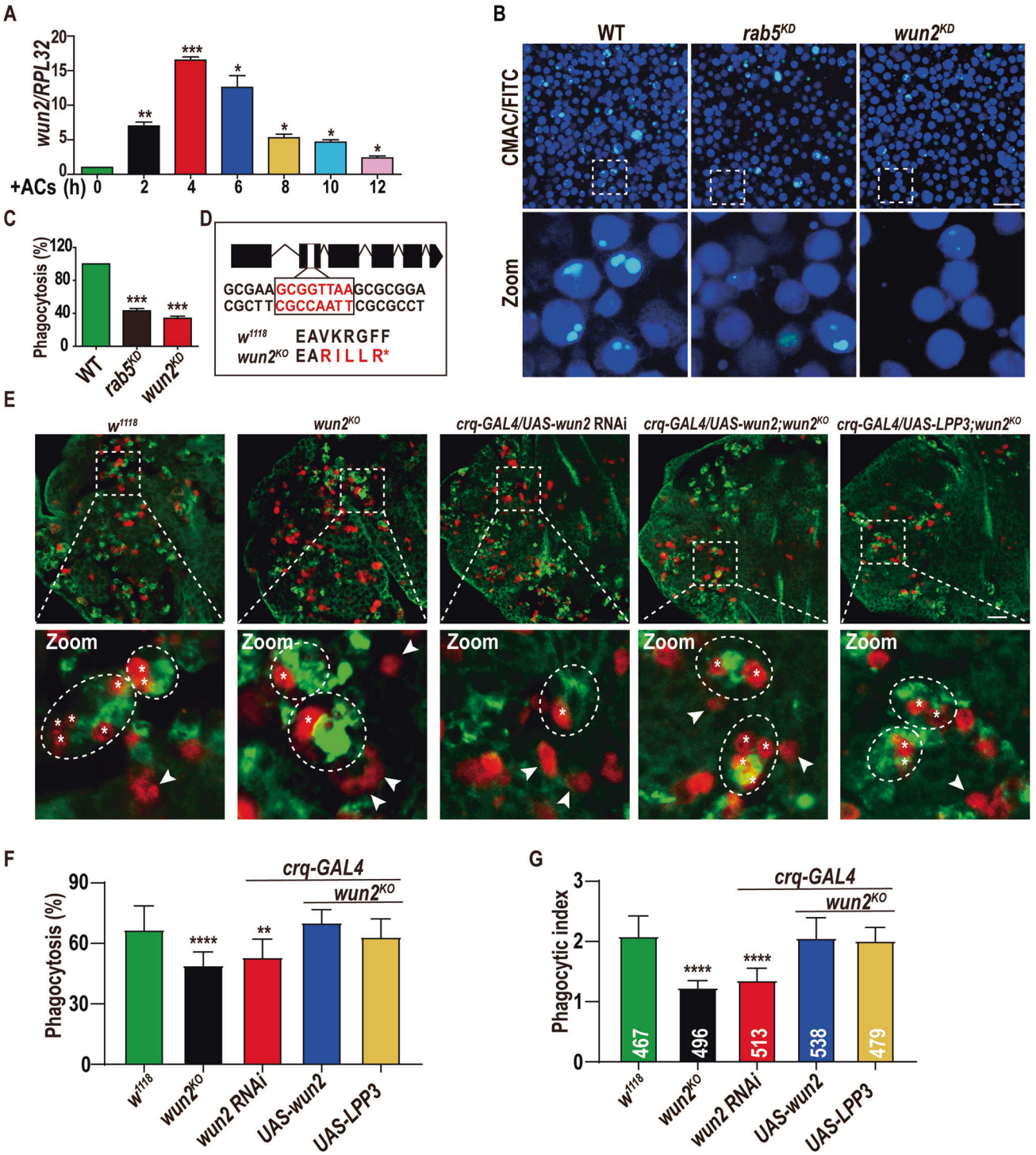


macrophages failed to engulf ACs efficiently (Fig. 2E and Supplementary Fig. 1B); the phagocytosis ratio (number of engulfed ACs compared to total ACs) decreased by 17.69% (Fig. 2F) and the average phagocytic index (average number of ACs per macrophage, PI) scores were lower than that in the wild-type (WT) embryo (Fig. 2G). The difference was observed in the *crq-GAL4*, *UAS-GFP* marker models; WT embryos showed ACs mostly inside macrophages, while in *wun2*$^{KO}$ embryos, most ACs were outside GFP-positive macrophages (Supplementary Fig. 1B–F). The hemocyte-specific knockdown of *wun2* using *crq-GAL4* led to a phenotype similar to that of the *wun2*$^{KO}$ mutant (Fig. 2E–G). Mutant macrophages that re-expressed *wun2* driven by *crq-GAL4* or *hml-GAL4* appeared to be fully rescued as most contained numerous ACs (Fig. 2E–G and Supplementary Fig. 3C–E). *Hemolectin (Hml)* is specifically expressed in embryonic and larval hemocytes, especially in plasmatocytes and crystal cells [27]. We found that *hml-GAL4* could drive *UAS-LifeAct-GFP* expression from stage 12 embryos to larvae (Supplementary Fig. 3A, B). In addition, the *wun2* mammalian homolog *LPP3* rescued the defective phenotypes in *wun2*$^{KO}$ (Fig. 2E–G and Supplementary Fig. 3C–E), indicating their functional conservation. Hence, *wun2* appears to be required for efferocytosis in *D. melanogaster*.

**Fig. 2 Macrophages of the *wun2* mutant show defective phagocytosis of ACs. A** The *wun2* mRNA levels were quantified using qRT-PCR following the addition of ACs for 2, 4, 6, 8, 10, and 12 h. 0 h S2 cells without ACs were used as the control group. Data are presented as mean ± SEM ($n = 3$ replicates, ANOVA; $^{*}p \le 0.05$; $^{**}p \le 0.01$; $^{***}p < 0.001$). **B** Phagocytosis of ACs (green) by S2 cells or *rab5* and *wun2* RNAi-treated S2 cells (blue). The *rab5*-RNAi S2 cells were used as positive controls. Scale bars: 50 μm. **C** Quantification of the experiments in **B**, with wild-type normalized to 100%. Bars show the phagocytosis percentage ± SEM (ANOVA; $^{***}p < 0.001$). **D** Schematic representation of *wun2* DNA (top), with blocks representing exons and broken lines representing introns. Eight-base pair-deletion at the sgRNA target resulted in a frameshift mutation (red) and premature termination codon (asterisk). **E** Macrophages and ACs of stage 13 embryos stained with Crq antibody (green) and Dcp-1 antibody (red) in $w^{1118}$, $wun2^{KO}$, *crq-GAL4/UAS-wun2* RNAi, *crq-GAL4/UAS-wun2;*$wun2^{KO}$, and *crq-GAL4/UAS-LPP3;*$wun2^{KO}$ embryos. The dashed box represents magnified subsequent panels, the arrows point to the ACs not engulfed, and circles indicate single macrophages. Scale bars: 20 μm. **F** Graph showing the number of engulfed ACs compared to total ACs for each genotype in **E**, and normalized as percentage ± SEM: $w^{1118}$ 66.42% ± 3.398, $wun2^{KO}$ 48.73% ± 1.949, *crq-GAL4/UAS-wun2* RNAi 52.75% ± 2.604, *crq-GAL4/UAS-wun2;*$wun2^{KO}$ 69.94% ± 1.885 and *crq-GAL4/UAS-LPP3* 62.83% ± 2.589. **G** Graph showing the mean PI ± SEM for each genotype in **E**. The number of quantified macrophages per genotype is indicated within each bar: $w^{1118}$ 2.080 ± 0.1091, $wun2^{KO}$ 1.227 ± 0.0384, *crq-GAL4/UAS-wun2* RNAi 1.349 ± 0.065, crq*l-GAL4/UAS-wun2;*$wun2^{KO}$ 2.051 ± 0.1446, *crq-GAL4/UAS-LPP3;*$wun2^{KO}$ 2.005 ± 0.0721. The statistical *p* values of **F** and **G** were obtained using one-way ANOVA, comparing all phenotypes to the wild-type ($^{**}p < 0.01$; $^{****}p < 0.0001$; ten embryos/genotype).

In *D. melanogaster*, hemocytes originate from the mesoderm of the head and develop into macrophages to disperse throughout the embryo; Even with severe manipulations of macrophage function can have relatively mild effects on its dispersal [28]. In the $wun2^{KO}$ mutant, macrophages developed normally and migrated throughout the embryos (Supplementary Fig. 4A, B and Videos 1 and 2). No differences were found in the number of macrophages at stage 13 between WT and $wun2^{KO}$ mutant flies (Supplementary Fig. 4C). The first wave of cell apoptosis began at stage 11 of embryogenesis and lasted until stage 16. There was no obvious difference in the number of ACs at stage 11 but AC counts were significantly higher in stages 14–15 of $wun2^{KO}$ embryos than in those of WT embryos (Supplementary Fig. 4A). And re-expression of *wun2* or *lpp3* in $wun2^{KO}$ could rescue the AC increased phenotype (Supplementary Fig. 4D). Therefore, we inferred that the higher ACs observed at stages 14-15 was caused by insufficient ACs clearance.

### *wun* is not required for efferocytosis

Previously, *wun* and *wun2* served as redundant genes to guide primordial germ cells [18, 29]. However, *wun* was excluded from the conditional RNA-sequencing data. To verify whether *wun* might nonetheless affect ACs clearance, we analyzed the location of Wun and Wun2 in S2 cells. They showed markedly different subcellular distribution in S2 cells (Fig. 3A, B). In contrast with *wun2*, *wun* knockdown did not affect ACs clearance in S2 cells (Fig. 3C, D). Furthermore, *wun* RNAi-treated embryos showed a level of phagocytosis that was almost equal to that of the WT embryos (Fig. 3E–G). In addition, double RNAi of *wun* and *wun2* did not exacerbated ACs clearance defects (Fig. 3E–G), suggesting the likelihood of their functional divergence in macrophages.

### Wun2 is not dependent on phosphatase activity for efferocytosis

Previous structural characterization revealed that the Wun2 catalytic site is located at the C-terminus of the acidPPc domain [14]. As the conserved domains are important for Wun2 catalytic activity in germ cell migration and maintenance [18], catalytic residues H274K, H326K, or double mutants (DM) were generated; Y225W was mutated as a control (Fig. 4A) [30, 31]. Subcellular localization revealed that Wun2-GFP fusion proteins typically appeared as punctate structures in the internal membrane, and to a less extent in the plasma membrane (Supplementary Fig. 5A). None of these mutations affected Wun2 localization in S2 cells (Supplementary Fig. 5A). Wun2 and Wun2 (DM) formed a ring-like structure around engulfed ACs (Fig. 4B), suggesting their potential role in the endosomal system. We purified Wun2 and its mutant proteins from transfected S2 cells (Supplementary Fig. 5B). Biochemical assays of Wun2 and its mutant proteins on phosphate esters indicated that the WT and control mutant Wun2 (Y225W) could dephosphorylate PA, C1P, LPA, and S1P in vitro (Supplementary Fig. 5C). In contrast, H274K and H326K mutants exhibited varying degrees of inhibited catalytic activity; Wun2 (DM) exhibited no phosphatase activity regardless of the substrate (Supplementary Fig. 5C), which is consistent with a previous study [30]. Additionally, re-expression of *wun2 (DM)* in the $wun2^{KO}$ mutant effectively rescued the ACs clearance defect (Fig. 4C–E), which indicated the participation of the catalytic site-null Wun2 in efferocytosis.

### Wun2 interacts with Rab11 in regulating efferocytosis

To identify the potential role of Wun2 in efferocytosis, a Flag-tagged-Wun2 stable S2 cell line was established. The Wun2-Flag protein was enriched by immunoprecipitation (Supplementary Fig. 6A), followed by liquid chromatography-tandem mass spectrometry (LC-MS/MS) (Supplementary Fig. 6B). Two-hundred ten proteins were identified as putative interaction partners of Wun2 (Supplementary Table 2). Based on the properties and distribution of Wun2 in cells, we selected a subset of endosome system proteins as strong potential interactors. RNAi suppression of *Rab11* led to significantly reduced efferocytosis efficiency (Supplementary Fig. 6C). Endosomal recycling routes have been classified in the literature as the 'fast recycling pathway,' regulated by Rab4, and the 'slow recycling pathway,' regulated by Rab11 [32]. Co-expression of Wun2 with Rab4 or Rab11, indicated that Wun2 was generally localized in the 'slow recycling pathway' (Supplementary Fig. 6D, F), and subsequent co-immunoprecipitation (co-IP) indicated that Wun2 interacted with the small GTPase Rab11 (Fig. 5A). Rab proteins cycle between the GTP-loaded state (active) and GDP-loaded state (inactive) [33]. Co-IP results revealed that Wun2 formed a complex with the active form of Rab11(Q70L) (Fig. 5B) but not with the dominant-negative Rab11(S25N) (Fig. 5C). This was further confirmed by the co-localization analysis of Wun2 with Rab11 (WT, Q70L, or S25N) in HeLa cells (Fig. 5D, E) and S2 cells (Supplementary Fig. 6E, F).

To address whether physical binding between Rab11 and Wun2 resulted in physiological effects in vivo, we characterized the efferocytosis phenotype of $rab11^{j2D1}$ and found that it failed to efficiently engulf ACs, with a lower phagocytosis ratio (Fig. 5F, G) and PI (Fig. 5F, H). In contrast, single heterozygous $wun2^{+/-}$ *or* $rab11^{j2D1+/-}$ mutant embryos were not distinguishable from the WT embryos; only embryos carrying the *wun2* and *rab11* double heterozygous combination exhibited defects in ACs clearance (Fig. 5F–H). These results suggested a genetic interaction between *wun2* and *rab11* to promote efferocytosis.

### Wun2 directly interacts with Rip11 and βv integrin to regulate efferocytosis

The immunoprecipitation assay of Wun2 and Rab11 showed that the interaction between these proteins was not very strong (Fig. 5A, B). The yeast two-hybrid assay performed to investigate whether Wun2 and Rab11 interacted with each other directly

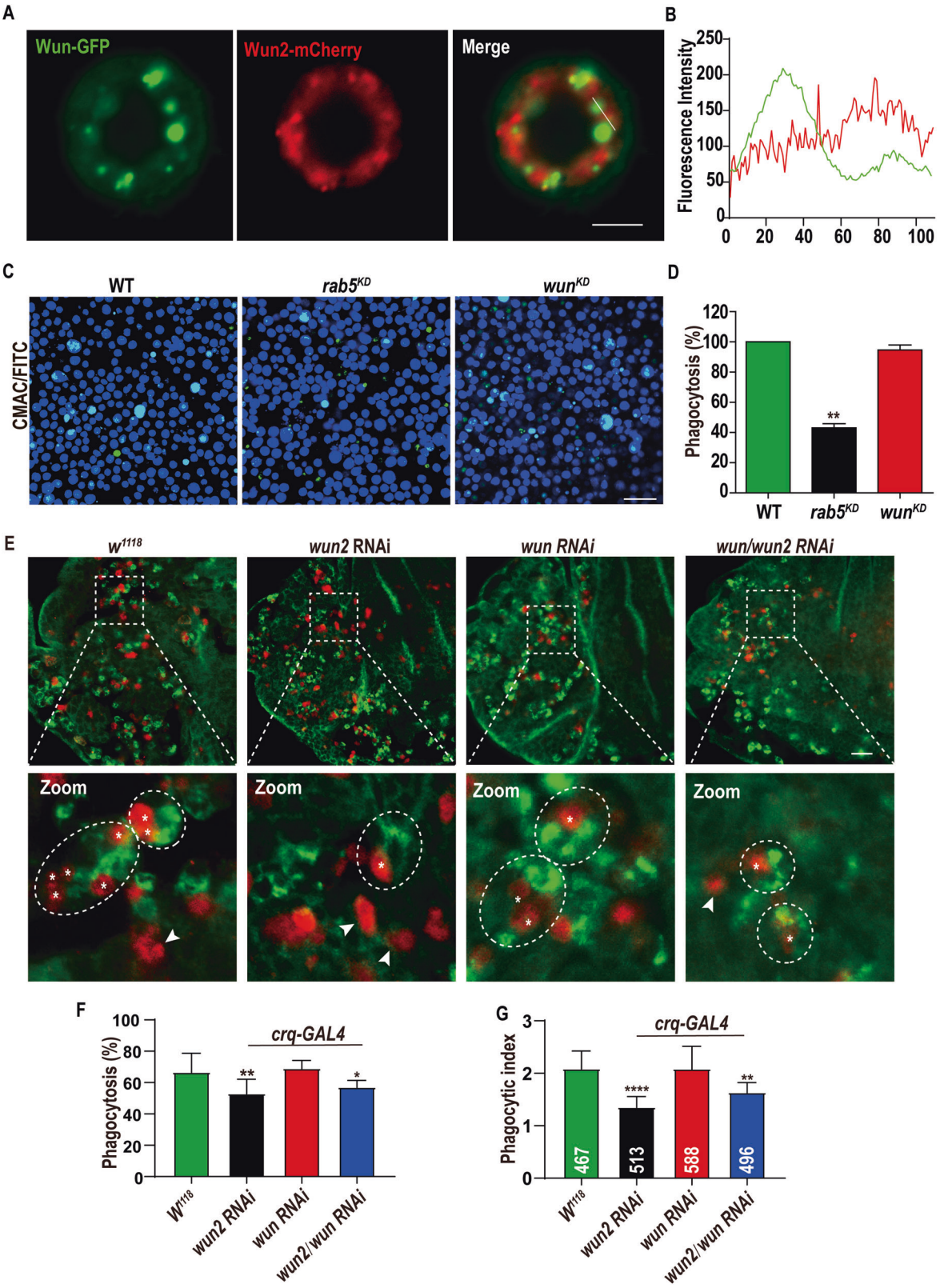


further revealed there was no interaction between these proteins, regardless of the forms of Rab11: WT, negative, or active (Fig. 6A). Hence, we hypothesized an indirect interaction between Wun2 and Rab11, likely through complex formation with other proteins. As the active Rab11 is reportedly capable of binding diverse effector proteins to regulate intracellular membrane traffic [34], we examined the possibility of a direct interaction between Wun2 and Rab11 effectors. Yeast two-hybrid analysis showed that Wun2 could directly interact with the Rab11 effector Rip11 (Fig. 6A). Co-localization and co-IP analyses revealed a strong interaction

**Fig. 3 *wun* does not affect ACs clearance for macrophages. A** S2 cells transfected with Wun-GFP and Wun2-mCherry vectors and visualized using fluorescence microscopy. Scale bar: 5 μm. **B** The fluorescence intensity of Wun (green) and Wun2 (red) from random lines traced in **A** was analyzed using ImageJ. **C** Phagocytosis of ACs (green) in wild-type or *wun* RNAi-treated S2 cells (blue). Scale bars: 50 μm. **D** Quantification of the phagocytosis ratio in **C**, using *rab5*-RNAi S2 cells as the positive control and normalizing the wild-type to 100% (ANOVA; $^{**}p < 0.01$). **E** Confocal micrographs of WT, RNAi-mediated knockdown of *wun2*, *wun* or double knockdown of *wun/wun2* in embryo macrophages, using a GAL4 driver with the promoter of *crq*. All embryos were stained with Crq (green) and Dcp-1 (red) antibodies. Scale bar: 20 μm. **F**, **G** Summary of the quantification of phagocytosis percentage and PIs of wild-type (66.42 ± 3.398, 2.08 ± 0.109), *wun2* RNAi (52.75 ± 2.604, 1.349 ± 0.06531), *wun* RNAi (68.84 ± 1.460, 2.079 ± 0.1372), and *wun/wun2* double RNAi (56.85 ± 1.259, 1.628 ± 0.06175) embryos. The number of quantified macrophages per genotype is indicated within each bar in **G**. Asterisks in **F** and **G** indicate statistical significance versus the wild-type (ANOVA; $^{*}p < 0.05$; $^{**}p < 0.01$; $^{****}p < 0.0001$). Bars represent the mean phagocytosis percentage ± SEM (error bars) (**F**) and PI ± SME (**G**), respectively.

between Wun2 and Rip11 (Fig. 6B–E). Furthermore, the catalytic site-null Wun2 mutant did not affect the interaction with Rip11 (Supplementary Fig. 7A). To narrow down the potential regions required for Wun2 and Rip11 interaction, we generated a series of systematic truncations of Wun2 (Wun2-1, 2, 3, 4, and 5) and Rip11 (Rip11-1, 2, 3, 4, 5, and 6) (Supplementary Fig. 7B) and found that the binding of Wun2-1 to the C2 domain of Rip11 (Rip11-5) was essential (Supplementary Fig. 7C). However, replacement of the Wun2-1 residues 155–177 with Wun2 C-terminal 345–350 residues, i.e., Wun2-1 (RC), resulted in the complete loss of interaction with Rip11 (Supplementary Fig. 7D), suggesting that residues 155–177 of Wun2 are essential for its binding to the C2 domain of Rip11.

Previous studies have demonstrated that mammalian LPP3 interacts with a subset of integrins to mediate cell functions [35, 36]. βv and αPS3 (scb) integrin subunits function as heterodimers in the regulation of ACs clearance and phagocytosis of *S. aureus* in *D. melanogaster* [12, 13]. We therefore investigated whether Wun2 could interact with αPS3 and/or βv integrin subunits and found a strong interaction between Wun2 and βv but not between Wun2 and αPS3 (Fig. 6A, F). Furthermore, the catalytic site-null Wun2 (DM) could still interact with βv (Supplementary Fig. 7A); the noncatalytic domain in Wun2-1 (Supplementary Fig. 7C), especially the region spanning the 116–134 residues, was required for Wun2 and βv interaction (Supplementary Fig. 7E). Hence, both Rip11 and βv integrin interact with the different residues of the noncatalytic domain of Wun2.

The suppression of βv or αPS3 integrin subunits in S2 cells led to an obvious reduction in ACs clearance (Supplementary Fig. 8A, B) and phagocytosis of *S. aureus* (Supplementary Fig. 8C, D); the *wun2*-RNAi-treated S2 cells also exhibited a significant decrease in the phagocytosis of bacteria (Supplementary Fig. 8C, D). The null allele $itgbn^{MB02607}$ mutant embryo failed to efficiently engulf ACs, exhibiting a phagocytosis rate of approximately 50.15% ± 2.519% (Supplementary Fig. 8E, F) and a PI of 1.233 ± 0.06043 (Supplementary Fig. 8E, G). These results are consistent with those of previous studies [12, 13, 37]. The hemocyte-specific knockdown of *rip11* or *βv subunit* using *crq-GAL4* caused a significant inhibition of ACs clearance in embryos (Fig. 6G–I). Double RNAi of *wun2* and *rip11* or *wun2* and *itgbn* in embryonic hemocytes exacerbated the ACs clearance defect (Fig. 6G–I). Heterozygous *wun2*/βv and $βv^{+/-}$;$rab11^{+/-}$ embryos also exhibited similar defects in ACs clearance (Supplementary Fig. 8E–G). These results provide strong evidence of genetic interactions among *wun2*, *rip11*, *rab11*, and *βv* for ACs clearance in embryonic macrophages. Importantly, the defects displayed by *wun2* and *βv* mutants could be rescued by the macrophage-specific expression of *βv* (Fig. 6J–L and Supplementary Fig. 8E–G).

## Wun2 is required for efficient recycling of βv

As mentioned above, Wun2 interacted with the recycling pathway proteins Rip11 and Rab11. As so, we hypothesized that *wun2* deficiency was likely to affect the recycling of βv integrin subunit to the macrophage surface. The $wun2^{KO}$ mutant displayed relatively low levels of βv integrin protein in whole-cell lysates (Fig. 7A, B) but the βv mRNA expression remained unchanged (Supplementary Fig. 9A). Immunofluorescent staining of embryos indicated that most βv integrin was distributed in the plasma membrane of WT macrophages whereas an uneven and aberrant aggregated pattern was displayed in the cytoplasm of $wun2^{KO}$ macrophages (Fig. 7C). Consistent with $wun2^{KO}$ mutants, the depletion of *rab11* induced relatively low levels of βv integrin (Supplementary Fig. 9B–E). In the $wun2^{KD}$ S2 cells, the abundant βv integrin was transported to the lysosomes (Supplementary Fig. 9F, G). When *wun2* RNAi cells were treated with the lysosomal acidification inhibitor chloroquine (CQ), the βv integrin levels were almost restored to that of the control cells (Fig. 7D, E). These results indicated that the loss of Wun2 resulted in routing βv integrin into the lysosomes, leading to its degradation.

The surface levels of transmembrane proteins are controlled by several processes, including protein synthesis, internalization, recycling, and degradation [38]. To determine whether the reduction of βv integrin in *wun2*-depleted cells results from inadequate recycling, we analyzed βv internalization and recycling by cell surface labeling with cleavable biotin [38, 39]. To determine βv internalization, the recycling pathways were inhibited with primaquine (PMQ). The βv integrin subunit was internalized with similar kinetics in *wun2*-knockdown ($wun2^{KD}$) and WT cells (Fig. 7F and Supplementary Fig. 9H). In contrast, the $wun2^{KD}$ cells showed a significant decreased recycling rate of βv to the plasma membrane (Fig. 7G and Supplementary Fig. 9I). We then isolated macrophages from larvae and labeled them with the βv integrin subunit antibody on the cell surface; degradation and recycling pathway were inhibited using CQ and PMQ, respectively, and the βv integrin antibody-labeled macrophages were allowed to perform endocytosis; however, less punctate βv integrin subunit-labeled macrophages were detected in $wun2^{KO}$ than in WT larvae, indicating that the βv integrin subunit is less distributed on $wun2^{KO}$ macrophage surfaces (Fig. 7H, I). Collectively, these data demonstrated that Wun2 facilitates the recycling of internalized βv integrin to the cell surface; therefore, the loss of Wun2 inhibits the recycling of internalized βv integrin, resulting in the lysosomal degradation of the receptor.

## Wun2 is an important regulator of integrin-mediated phagocytosis

Live cell tracking of efferocytosis could uncover multiple qualitative and quantitative features of coordinated clearance of apoptotic corpses [40]. Macrophages are highly motile cells that can dynamically alter their actin cytoskeleton to perform migration and phagocytosis. They use their actin-rich lamellipodia and filopodia to engulf ACs [41]. As the active state of integrin leads to the remodeling of the actin cytoskeleton [42], the insufficient expression of the βv integrin subunit in the $wun2^{KO}$ mutant resulted in the disorganized actin cytoskeleton of macrophages, with smaller and fewer pseudopodia near the leading edge (Fig. 8A–D). In contrast, WT macrophages had rich branched F-actin meshes with large lamellipodial and filopodial protrusions (Fig. 8A–D). We injected fluorescent Annexin V into

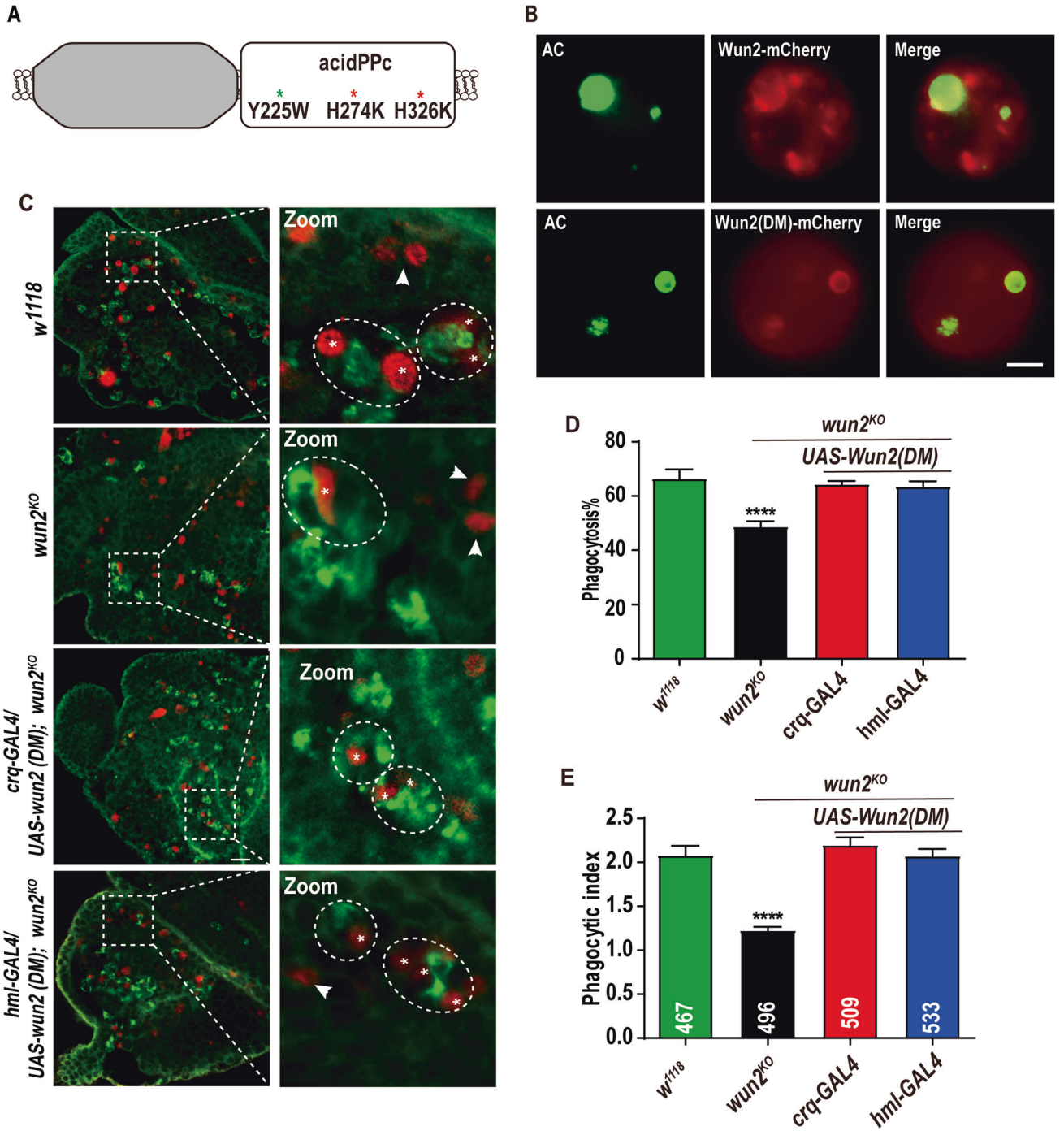


**Fig. 4 Wun2 catalytic activity is not required for efferocytosis. A** Structure of the Wun2 protein. Left, the noncatalytic domain (gray); Right, the catalytic domain acidPPc (white); the putative catalytic residues of Wun2, His 274 or His 326, were mutated into Lys (H274K and H326K, the catalytically dead mutants are indicated by red asterisks), the non-conserved residue Tyr 225 was mutated into Trp (Y225W, green asterisk). **B** S2 cells transfected with Wun2-mCherry or Wun2 (DM)-mCherry, containing the double point mutation (DM) of His 274 and His 326 into Lys, and incubated with FITC-labeled ACs (green) to analyze Wun2 location after engulfing ACs. Scale bar: 5 μm. **C** Projected confocal micrographs of Crq (green) and Dcp-1 (red) antibodies-stained stage 13 embryos of $w^{1118}$, $wun2^{KO}$ homozygous, and *UAS-wun2 (DM)* were expressed in $wun2^{KO}$ macrophages under the control of *crq-GAL4* or *hml-GAL4* drivers. Scale bars: 20 μm. **D** Summary of the quantification of phagocytosis percentage in **C**, the phagocytosis ratios of $w^{1118}$, $wun2^{KO}$, *crq-GAL4/UAS*-wun2 (DM);$wun2^{KO}$, and *hml-GAL4/UAS*-wun2 (DM);$wun2^{KO}$ were 66.42% ± 3.398, 48.73% ± 1.949, 64.39% ± 1.176, and 63.47 ± 1.932, respectively. Bars represent the phagocytosis mean percentage ± SEM (ANOVA; ****$p < 0.0001$). **E** PI in: $w^{1118}$], 2.080 ± 0.1091; $wun2^{KO}$, 1.227 ± 0.03844; *crq-GAL4/UAS*-wun2 (DM);$wun2^{KO}$, 2.170 ± 0.1247; and *hml-GAL4/UAS-wun2 (DM);*$wun2^{KO}$, 2.073 ± 0.08031. The number of quantified macrophages per genotype is indicated within each bar. Bars represent mean PI ± SEM (error bars) (ANOVA; ****$p < 0.0001$).

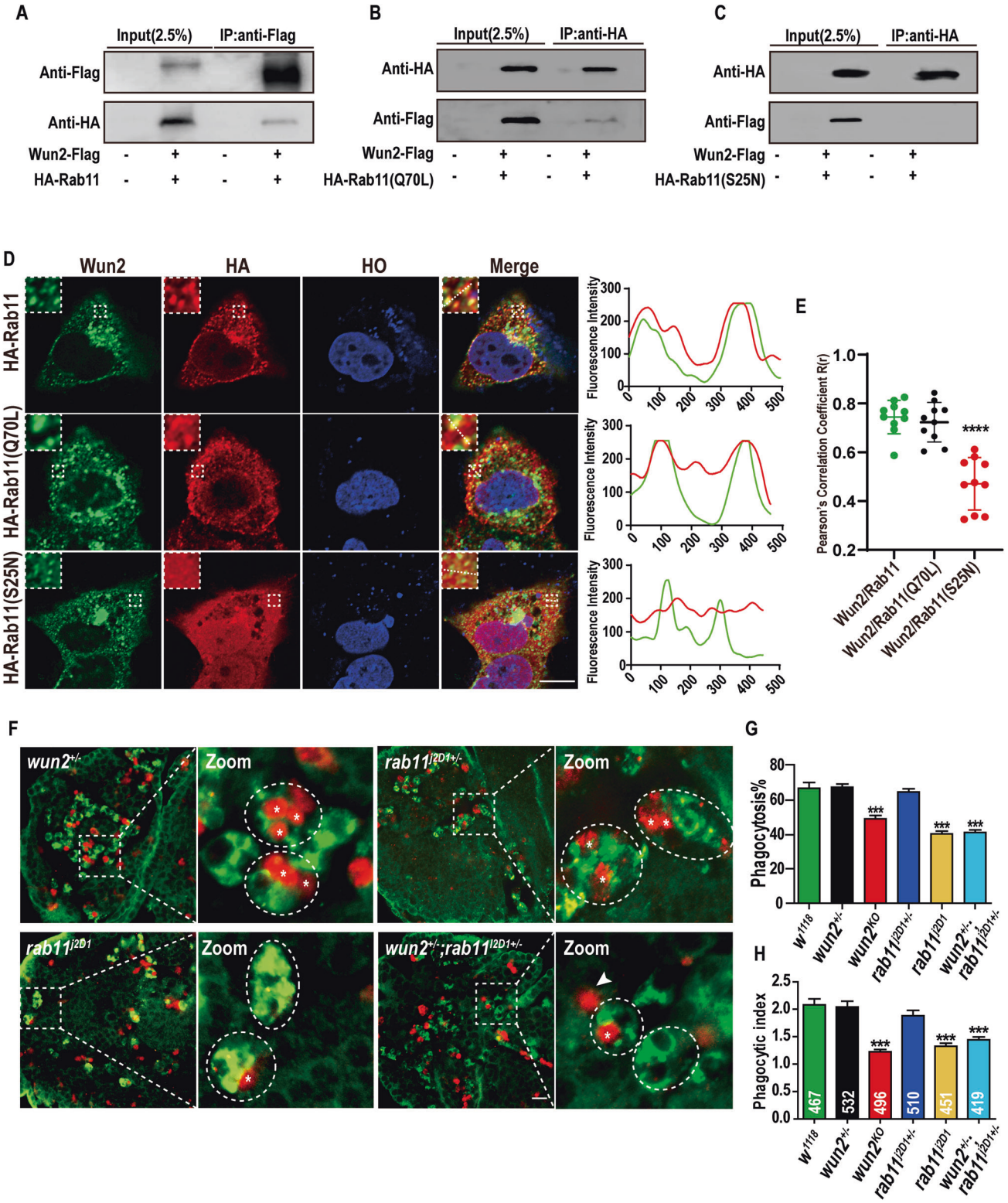


the ventral side of *D. melanogaster* embryos between the overlying epithelium and the central nervous system. In vivo imaging revealed that WT macrophages used their actin-rich lamellipodia and filopodia to envelop Annexin-V labeled ACs (Fig. 8B, E and Supplementary Video 3). The *wun2* and *itgbn* mutant macrophages showed a significantly reduced pseudopodia structure. The lamellipodial protrusions of *wun2* hemocytes were undynamic, thus affecting the ability of hemocytes to capture ACs (Fig. 8E, F and Supplementary Video 4).

## DISCUSSION

Removal of cellular corpses is important in both homeostasis and disease. Defective efferocytosis has been implicated in a variety of

**Fig. 5 Wun2 interacts with active Rab11 to regulate ACs clearance. A** Flag-tagged Wun2 associated with HA-tagged wild-type Rab11 in S2 cells; Co-IPs were performed with anti-Flag M2 Affinity Gel on lysates of S2 cells co-expressing Wun2-Flag and HA-Rab11. The precipitated proteins were detected using western blot with Flag and HA antibodies, respectively. **B**, **C** Co-transfected Flag-tagged Wun2 with HA-tagged active Rab11 (Q70L, the residue Gln70 was mutated into Leu) or HA-tagged negative Rab11 (S25N, the residue Ser 25 was mutated into Asn) in S2 cells. Co-IPs were performed with anti-HA magnetic beads and precipitates were detected using immunoblotting assays with antibodies for HA and Flag, respectively. A total of 2.5% of the crude extracts were loaded to ensure they were expressed in the co-transfected cells. Results are representative of at least three independent experiments. **D** HeLa cells co-transfected wun2-GFP with wild-type or mutant HA-rab11. Immunofluorescence was detected using anti-HA (red) antibodies; nuclear staining was performed with Hoechst (blue). The intensity profile from random lines traced through the reticular cytoplasmic area was analyzed using ImageJ. Scale bar: 10 μm. **E** Quantification of the colocalization of Wun2 with wild-type Rab11, active Rab11 (Q70L) or negative Rb11 (S25N) using the Pearson's correlation coefficient (0.7444 ± 0.02169, 0.7233 ± 0.02559 and 0.4711 ± 0.03388, respectively). Values from ten cells are represented as mean ± SEM, comparing all the genotypes to the Wun2/Rab11 (ANOVA; ****$p < 0.0001$). **F** The single heterozygous embryos or homozygous embryos of *wun2* and *rab11*, and the double heterozygous embryos, were stained with Crq antibody (green) and Dcp-1 antibody (red). The arrow points to ACs not engulfed; circles outline single macrophages. Scale bars: 20 μm. **G** Summary of the phagocytosis percentage: $w^{1118}$ 66.42% ± 3.398; heterozygous $wun2^{KO}$ 67.02% ± 1.838; heterozygous $rab11^{j2D1}$ 64.27% ± 1.833; homozygous $wun2^{KO}$ 48.73% ± 1.949; homozygous $rab11^{j2D1}$ 40.11% ± 1.524; and double heterozygous *wun2* and *rab11* 40.82% ± 1.563, (ANOVA; ***$p < 0.001$). **H** Quantification of the PI yielded the following values: $w^{1118}$ 2.080 ± 0.1091, heterozygous $wun2^{KO}$ 2.043 ± 0.1054, heterozygous $rab11^{j2D1}$ 1.882 ± 0.09789, homozygous $wun2^{KO}$ 1.227 ± 0.1216, homozygous $rab11^{j2D1}$ 1.327 ± 0.05582, and double heterozygous *wun2* and *rab11* 1.443 ± 0.0543. The number of quantified macrophages per genotype is indicated in each bar; significant differences were compared to $w^{1118}$ (ANOVA; ***$p < 0.001$). Error bars represent SEM.

autoimmune and inflammatory diseases [4, 43–45]. Based on RNA-sequencing analysis, we attempted to identify novel genes that were involved in efferocytosis and their potential applicability in the discovery of novel treatments for diseases driven by defective efferocytosis. We identified a candidate gene, *wun2*, which acts as a regulator in macrophages to clear ACs. Wun2 participates in the Rab11-regulated recycling pathway, facilitating the recycling of the βv integrin subunit from endosomes to cell membrane surfaces, allowing the rearrangement of F-actin-rich lamellipodia and filopodia to envelop ACs (Fig. 8G).

The *D. melanogaster* LPPs Wun and Wun2 play a significant role in regulating the survival and migration of germ cells, and they have been reported to act redundantly in somatic cells and germ cells [17, 29–31, 46]. In a previous study using single-cell RNA-sequencing to map hemocytes across different inflammatory conditions in *D. melanogaster* larvae [47], we found that Wun2 were enriched in most hemocyte clusters. The mammalian homolog of Wunens (LPP3) is important in immune response; it allows for the efficient exportation of mature T cells from the thymus into circulation. The conditional deletion of LPP3 in epithelial cells or endothelial cells is sufficient to inhibit T cell egress [48]. However, the exact functions of LPP3 or Wunens in macrophages have not been studied. In contrast with germ cells and somatic cells, a previous study found that the localization and function of Wun and Wun2 differed in the trachea, which is consistent with the present results. Wun and Wun2 seem to play different roles in macrophages; while the loss of Wun2 leads to efferocytosis defects, Wun is not required for this process, supporting these LPPs function autonomously in the different tissues [19]. The phosphatase activities of Wunens are crucial for germ cell and caudal visceral mesoderm cell migration and survival [30, 31, 49]. In addition to its phosphatase activity, LPP3 exhibits noncatalytic effects at the cell surface [35, 36]. The transgenic expression of catalytic-site-null Wun2 in $wun2^{KO}$ macrophages could rescue the defects in ACs clearance, demonstrating the diversity of Wun2 functions in the different cells. Therefore, we hypothesized efferocytosis may be independent of the Wun2 phosphatase activity in macrophages. However, various phosphatases synergize inside the organism, and whether other enzymes complement the catalytic function of Wun2 remains to be studied.

The subcellular localization of LPP3 is dynamic and cell-specific to the endoplasmic reticulum, endosomes, vesicular structure, or Golgi complex [50, 51]. Wun2 mainly localized to the intracellular membrane and interacted with GTP-loaded Rab11 in *D. melanogaster* macrophages. Rab11 is a GTPase localized to several intracellular membrane compartments, including endosomes and nascent phagosomes [52, 53]. Rab11 participates in the mobilization and recruitment of early endocytic compartments in macrophages to enhance phagocytosis and ACs clearance [53, 54]. Integrin subunits βv and αPS3 function as a heterodimer in regulating ACs clearance and *S. aureus* engulfment by phagocytes [12, 13]. Unlike many other cell surface receptors that undergo synchronized ligand-induced internalization and degradation, internalized integrin receptors that enter early endosomes can be recycled back to the plasma membrane directly from peripheral early endosomes via Rab4-regulated or Rab11-regulated pathways [23, 55, 56]. For example, the recycling of β1 integrin depends on SNX17 or SNX31 binding to sort integrin into recycling vesicles [57, 58]; VPS3 and VPS8 control β1 integrin trafficking [56]. The diverse functions of Rab11 are mediated by its effector proteins, which appear to operate as adaptor molecules to recruit various regulatory membrane transport proteins [59]. Rip11 is an effector for Rab11 that preferentially associates with the GTP-bound Rab11, regulating apical membrane trafficking via recycling endosomes in polarized epithelial cells [59]. Rip11 comprises a C2 domain, which is found in several proteins that serves as the protein–phospholipid or protein–protein binding modules involved in protein translocation to a specific region [60]. For example, the binding of the C2 domain to anionic phospholipids mediates the rapid translocation of protein kinases C to the plasma membrane [61]; the C2 domain of cytosolic phospholipase A2 is necessary and sufficient for its translocation to the nuclear envelope upon calcium ion influx [62]; the interaction of Rip11 C2 domain with neutral phospholipids is important for protein trafficking from recycling endosomes to the apical plasma membrane [59, 63]. The present study showed that the C2 domain is also important for the interaction of Rip11 with Wun2.

Mammalian LPP3 interacts with a subset of integrins to mediate cell–cell adhesion and functions [35, 36]; Wun2 is highly similar to LPP3, showing a strong interaction with integrin subunit βv. Accumulating evidence suggests that integrins connect the extracellular matrix to the cytoskeleton, allowing phagocytic cells to adjust F-actin-containing protrusions, including lamellipodia and filopodia [41, 42, 64]. Macrophages use two distinct modes of engulfment: lamellipodial and filopodial phagocytosis [41]. We concluded that Wun2 physically interacts with the Rip11 C2 domain and integrin subunit βv; Wun2 and Rip11 function in the Rab11 pathway to regulate the recycling of integrin subunit βv to the plasma membrane; Wun2 depletion increases βv integrin subunit transport to lysosome, resulting in its insufficient distribution on the cell surface of macrophages and thus to insufficient generation of lamellipodia and filopodia for engulfing ACs. However, the possible participation of Wun2 in modifying the endosomal membrane is unclear. Further research is required to determine whether Wun2 and Rip11 regulate the stability of integrin subunit βv to bind to endosomal membranes, or the

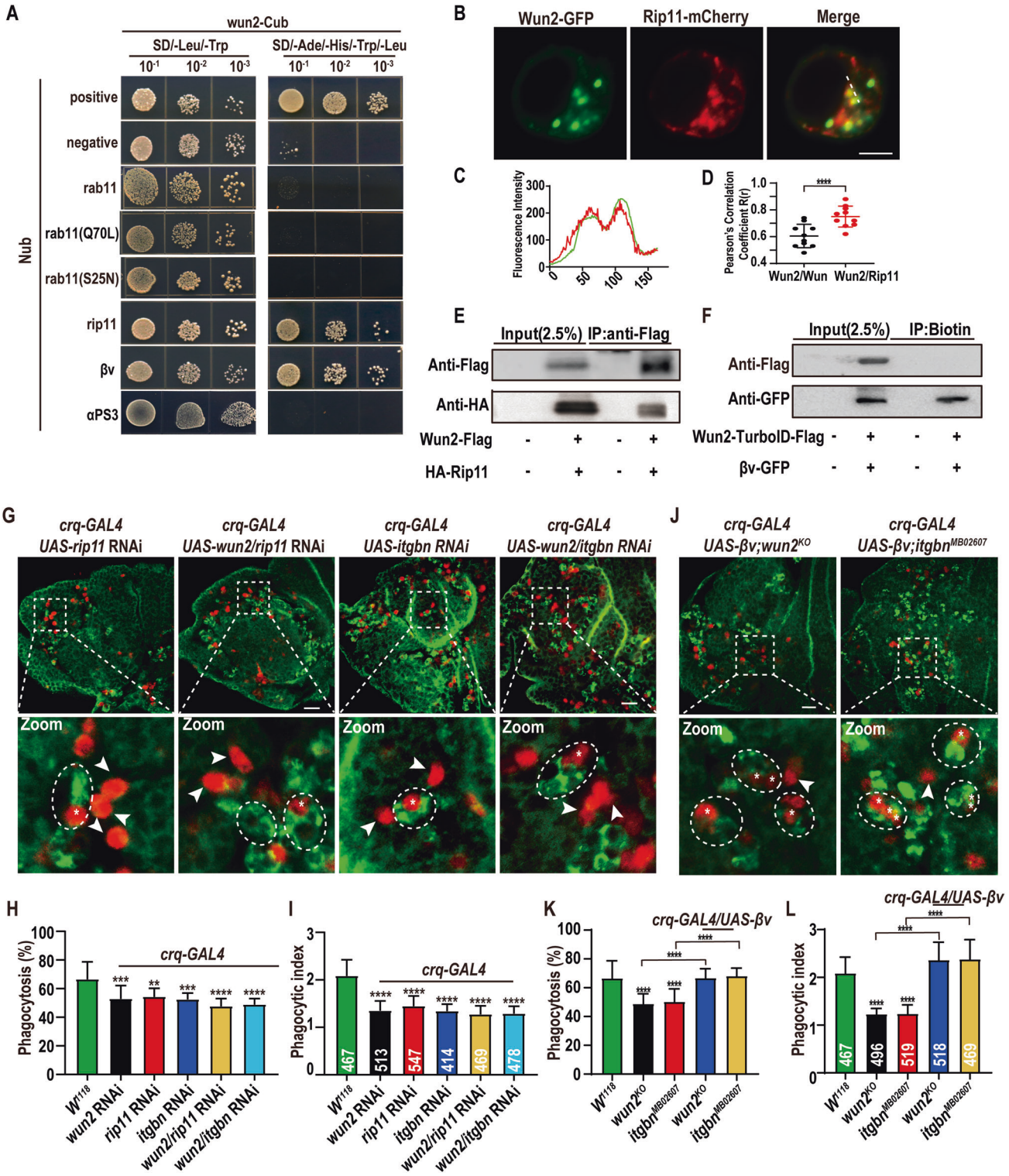


budding and fission of endosomal lipid membranes, or bind to selective phospholipids to enrich these membranes.

## MATERIALS AND METHODS

### Cell culture and cell transfection

*Drosophila melanogaster* S2 cells were cultured in Sf-900TM II SFM (Gibco # 10902088) or Schneider's *Drosophila* Medium (Gibco # 21720001) with 50 U/mL penicillin and 50 μg/mL streptomycin at 25 °C. S2 cells were then transfected with Fugene HD reagent (Promega # E2311) for transient expression or selected with 5 μg/mL puromycin to generate stable S2 cell lines. HeLa cells were grown at 37 °C and 5% $CO_2$ in Dulbecco's modified Eagle medium (Gibco # 11965175) supplemented with 10% fetal bovine serum, 1% penicillin, and 1% streptomycin. Additionally, cells were transfected with Lipofectamine™ 2000 (Thermo # 11668019). All the cell lines were confirmed by ATCC via short tandem repeat profiling and expanded at low passages and stored in liquid nitrogen after receipt. Cells were used within ten passages for experiments or resuscitated within 1 month.

**Fig. 6 Wun2 directly interacts with Rip11 and βv integrin subunit to regulate ACs clearance. A** Yeast two-hybrid assays to detect Wun2 (bait) interaction with prey proteins Rab11, positive Rab11(Q70L), negative Rab11(S25N), Rip11, integrin subunits βv and αPS3. Different concentrations of the labeled yeast transformants were assayed on SD-Ade-His-Trp-Leu plates. The empty NubWt and NubG vectors served as positive and negative controls, respectively. **B** Co-localization of Rip11-mCherry with Wun2-GFP in S2 cells. Scale bar: 5 μm. **C** The fluorescence intensity of Wun2 (green) and Rip11 (red) from random lines is shown. **D** Quantification of the colocalization of Wun2 with Wun (Fig. 3A) or Wun2 with Rip11 using Pearson's correlation coefficient (0.6050 ± 0,02762 and 0.75 ± 0.02481 respectively). Values from ten cells are represented as mean ± SEM (Student's *t* test; ****$p < 0.0001$). **E** Co-IP analysis of the interaction between Wun2-Flag and HA-Rip11. Precipitates were performed with anti-Flag M2 Affinity Gel and detected by western blot (WB) with antibodies for HA and Flag. 2.5% of the crude extracts were loaded. **F** Proximity labeling for detecting Wun2 and βv integrin subunit interaction. Wun2 was fused with TurboID and Flag as the bait protein. The co-expression of Wun2-TurboID-Flag and βv-GFP S2 cells labeled with 50 μM biotin was analyzed. Streptavidin-coated magnetic beads were used to capture the biotinylated proteins. The βv integrin subunit was labeled by Wun2-turboID-Flag and could be detected by WB. Three independent experiments were repeated. **G** Confocal micrographs of RNAi-mediated knockdown of *rip11*, *itgbn*, or double knockdown of *wun2/rip11*, *wun2/itgbn* in embryo macrophages, using a GAL4 driver with the promoter of crq. All embryos were stained with Crq (green) and Dcp-1 (red) antibodies. Scale bar: 20 μm. **H** Phagocytosis percentages: $w^{1118}$ 66.42% ± 3.398 [8]; *wun2* RNAi, 52.75% ± 2.604; *rip11* RNAi 54.17 ± 1.671; *itgbn* RNAi 52.34 ± 1.261; *wun2* and *rip11* double RNAi 45.21 ± 1.465; and *wun2* and *itgbn* double RNAi 45.69 ± 0.8877. Bars represent the phagocytosis mean percentage ± SEM, (ANOVA; **$p < 0.01$; ***$p < 0.001$; ****$p < 0.0001$). **I** Quantification of PI: $w^{1118}$ 2.080 ± 0.109; *wun2* RNAi 1.349 ± 0.653; *rip11* RNAi 1.443 ± 0.069; *itgbn* RNAi 1.339 ± 0.04725; *wun2* and *rip11* double RNAi 1.161 ± 0.03311; and *wun2* and *itgbn* double RNAi 1.142 ± 0.03241 (ANOVA; ****$p < 0.0001$). **J** Macrophages and ACs stained with Crq antibody (green) and Dcp-1 antibody (red), under the control of *crq-GAL4*, *wun2* and *βv* mutant embryos specifically expressed βv integrin subunit in the macrophages. Scale bars: 20 μm. **K**, **L** Summary of the quantification of phagocytosis percentages and PIs of wild-type (66.42 ± 3.398, 2.08 ± 0.109), $wun2^{KO}$ (48.73 ± 1.949, 1.227 ± 0.03844), $itgbn^{MB02607}$ (50.15 ± 2.519, 1.233 ± 0.06043), *crq-GAL4/UAS-βv;*$Wun2^{KO}$ (66.60 ± 1.841, 2.359 ± 0.1192), and *crq-GAL4/UAS-βv;*$itgbn^{MB02607}$ (68.03 ± 1.557, 2.377 ± 0.1304) embryos. The number of quantified macrophages per genotype is indicated within each bar in **L**. Asterisks indicate statistical significance, $wun2^{KO}$ and $itgbn^{MB02607}$ mutants were compared to wild-type (ANOVA; ****$p < 0.0001$). Error bars represent the SEM of phagocytosis mean percentage (**K**) and mean PI (**L**).

## Antibody generation

The anti-integrin subunit βv and anti-Wun2 antibodies were obtained by immunizing mice in our lab; the integrin βv immune protein fragment consisted of 1–360 amino acids and Wun2 was prepared by fusing the amino acid fragments 1–75 and 231–265, which were expressed in *Escherichia coli* as a glutathione S-transferase-fused protein and then purified. The generation and use of anti-Crq antibodies have been reported in a previous study [10].

## RNA-sequencing analysis

Total RNA samples were extracted from S2 cells using the Direct-zol RNA miniprep kit (Zymoresearch #R2052) and reverse-transcribed using the Transcriptor First Strand cDNA Synthesis Kit (Roche #04896866001). RNA-sequencing was performed by Annoroad Corporation using a HiSeq 2500 platform (Illumina) for determining differential gene expression. Raw reads containing adapters, poly-N, and low-quality reads were filtered, and the effective data were mapped to the *D. melanogaster* reference genome using TopHat (version 2.0.12) [65]. After excluding ribosomal and transfer RNA, we estimated the gene expression based on FPKM. The *p* values were adjusted using the Benjamini and Hochberg method [66]. All RNA-seq data files are available from the NCBI SRA database (accession number PRJNA721223). The URLs is https://www.ncbi.nlm.nih.gov/Traces/study/?acc=PRJNA721223&o=acc_s%3Aa.

## Double-stranded RNA production and RNAi treatment

Primer sequences used to generate specific double-stranded RNA (dsRNA) were obtained from the *D. melanogaster* RNAi Screening Center (DRSC) DRSC/TRiP Functional Genomics Resources (harvard.edu) and were predicted to have no off-targets and primers with T7 RNA polymerase binding sites at the 5′ end. Amplicons were obtained by PCR under the following conditions: 94 °C for 2 min; 30 cycles of 94 °C for 15 s, 56 °C for 30 s, and 68 °C for 45 s; and 10 min extension at 68 °C. dsRNA was generated using 1 μg of amplicon and a High Yield RNA Synthesis Kit (NEB #E2040S) for dsRNA synthesis. The dsRNA sequences are presented in Supplementary Table 3.

## RNA preparation and quantitative real-time PCR

For quantitative analysis of gene expression, total RNA was extracted from S2 cells using the TRIzol reagent (Invitrogen #15596026) and the Direct-zol RNA miniprep kit (Zymoresearch #R2052). One microgram of RNA was reverse-transcribed with the Transcriptor First Strand cDNA Synthesis Kit according to the manufacturer's instructions (Roche #04896866001). Quantitative real-time PCR was performed using cDNA, primers (Supplementary Table S3), and the SYBR Mix (Roche #04707516001) in ABI StepOne system (Perkin-Elmer). All experiments were performed in triplicate with mRNA samples extracted from at least three biological replicates. Relative gene expression was determined based on the cycle threshold value and normalized to that of the *rpl32* gene.

## In vitro S2 cell phagocytosis assay

As described in previous studies [67, 68], S2 cells were incubated with 0.25 μg/mL actinomycin D (Sigma #SBR00013) in a culture medium for 18 h, fixed in 10% formaldehyde, and resuspended in serum-free medium (SFM) at a concentration of $10^7$ cells/mL. Next, 1 mL ACs were treated with 5 μg/mL fluorescein-5-isothiocyanate (FITC, Thermo Fisher #F1906) and rotated for 1 h away from light to ensure even dispersion. The cells were then washed twice with SFM and resuspended in 1 mL SFM; FITC-labeled ACs were added to live S2 cells at a ratio of 10:1 and incubated for 6 h. Cells were counterstained with 25 mM CellTracker™ Blue CMAC Dye (Thermo Fisher #C2110) for 1 h and then gently washed with phosphate-buffered saline (PBS); 0.4% trypan blue (Gibco, #15250061) was added to quench the fluorescence of non-phagocytic ACs. The proportion of S2 cells containing ingested ACs was determined by inverted fluorescence microscopy or flow cytometry, and the ratio of double-labeled live cells to all live cells was calculated as a percentage.

For the bacterial phagocytosis assays, the *S. aureus* strain RN4220 was transformed with the plasmid pRN11, which expresses the red fluorescent protein. The *S. aureus* cells were grown with constant aeration at 37 °C with B2 broth until they reached an optical density of 0.4–0.6 at 600 nm. The cells harvested from the B2 broth were centrifuged at 8000 × *g* for 10 min at 20 °C and then washed three times with deionized water and resuspended in 1 mL Sf-900TM II SFM medium. S2 Cells were plated at a density of $1 \times 10^6$ cells/well in a 96-well plate and incubated for 6 h with 20 μL of the *S. aureus* culture. After this period, cells were mounted in Vectashield medium (Vector Laboratories) and observed on a confocal microscope (C2, Nikon instruments) using a 20× objective.

## Fly strains and genetics

The following *D. melanogaster* strains were obtained from the Bloomington Stock Center: $Rab11^{j2D1}$, *hml -GAL4*, $Itgbn^{MB02607}$, $wun2^{TKO.GS01135}$, *vasa–cas9*, *UAS-LifeAct-GFP*, *srpHemo-Moe-3×mCherry*, *UAS-GFP* (IDs: 12148, 6395, 24022, 77295, 51323, 57326, and 35786). *Crq-GAL4* (III) was a gift from Dr. Zongzhao Zhai. The following *D. melanogaster* RNAi strains were obtained from the Tsinghua Fly Center: *rip11* (THU3832), *βv* integrin (THU0442), *wun* (THU0875), and *wun2* (THU0869). The vectors *pUAS-wun2*, *pUAS-βv* integrin, *pUAS-wun2* (DM), and *pUAS-LPP3* were constructed in our lab. Briefly, selected genes were amplified by PCR and cloned into the Invitrogen pENTR/D-TOPO vector (Thermo Fisher #K242020). The Gateway™ LR Clonase™ II kit (Thermo Fisher #11791100) was used to move selected genes from vector pENTR/D-TOPO to pPWG following the manufacturer's instructions. Transgenic lines were generated using the PhiC31-targeted integration system by Unihuaii Inc. All *D. melanogaster* stocks were maintained in incubators at 25 °C, unless otherwise indicated. The $wun2^{KO}$ mutant line was generated by crossing the transgenic female $wun2^{TKO.GS01135}$ with *vasa–cas9* males. *vasa-cas9/+;sgRNA-wun2/+* flies were crossed with a Sp/CyO balancer strain. Based on heredity laws, we selected gene knockout flies.

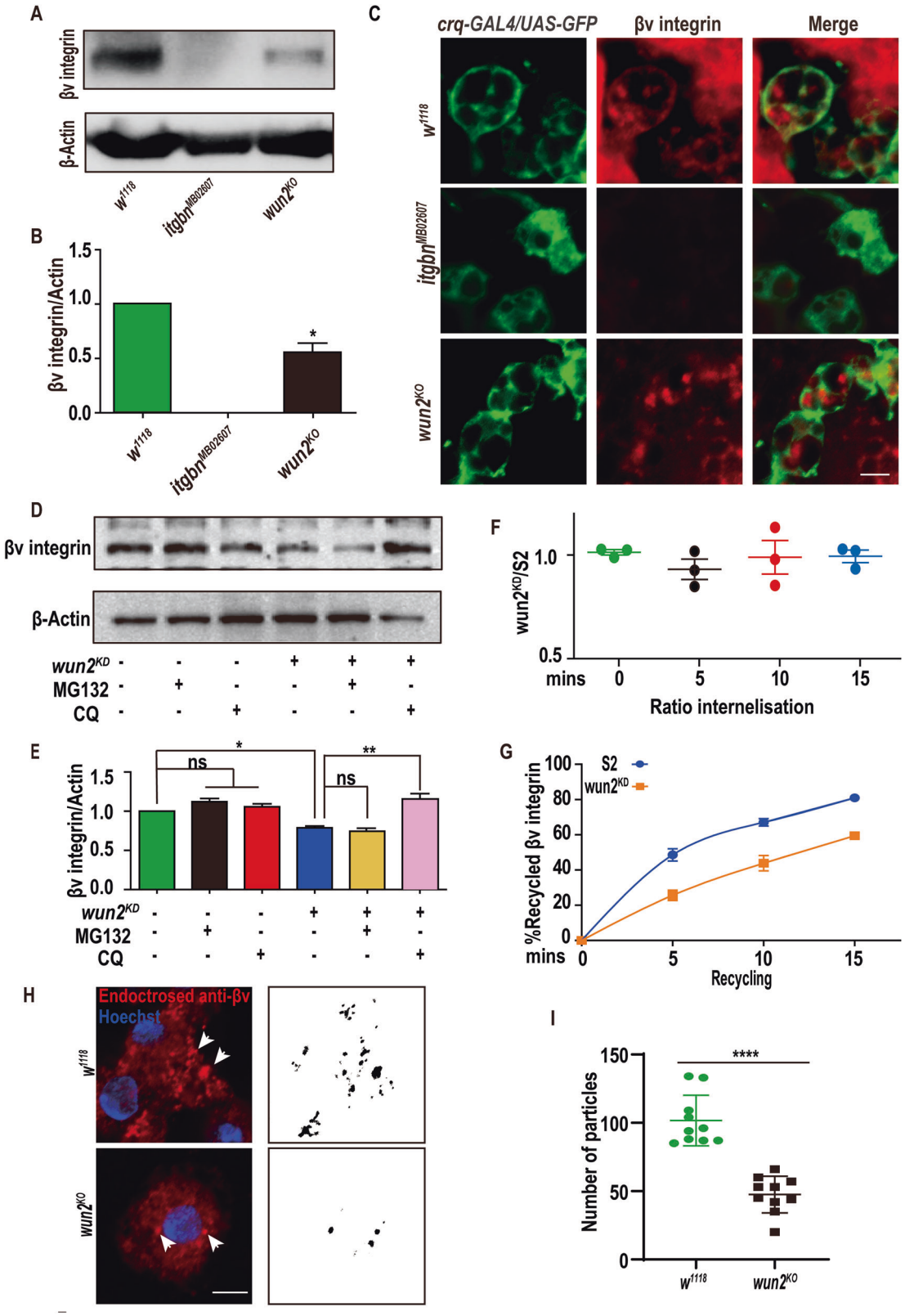


**Protein extraction and western blotting**

Protein samples were extracted and homogenized on ice in lysis buffer (50 mM Tris-HCl [pH 7.4], 1% TritonX-100, 0.15 M NaCl, 1 mM EDTA) with protease inhibitors. Lysates were centrifuged at 10,000 × *g* for 30 min, and the supernatants were collected and quantified using the bicinchoninic acid assay. Equal protein amounts were separated using electrophoresis and transferred to polyvinylidene difluoride membranes, which were blocked and incubated overnight with primary and secondary antibodies coupled with peroxidase. The antibodies were used at the following dilutions: mouse anti-actin (CST), 1:1000; mouse anti-Flag (Sigma) 1:1000; mouse anti-HA (CST) 1:1000; mouse anti-GFP 1:1000, mouse anti-Wun2 1:500, mouse anti-βv integrin 1:500, and secondary antibodies 1:10 000 (all

**Fig. 7 Wun2 protects βv integrin from degradation by sorting the recycling pathway. A** Western blot analysis of βv integrin expression levels in $w^{1118}$, $itgbn^{MB02607}$, and $wun2^{KO}$ *D. melanogaster*. β-actin was used as the loading control. **B** Quantification of βv integrin subunit expression levels in **A**, ($n = 3$ replicates). Asterisks indicate statistical significance versus $w^{1118}$ (ANOVA; $^{*}p < 0.05$). Data are presented as mean ± SEM. **C** Confocal micrographs of GFP-expressing wild-type, *itgbn* mutant and *wun2* mutant embryo macrophages under the control of *crq-GAL4*. Embryos were labeled with βv integrin antibody (red). Scale bars: 10 μm. **D** Western blot analysis of the expression of βv integrin in wild-type or *wun2* RNAi S2 cells, treated with either proteasome inhibitor MG132 (0.5 μm) or lysosome inhibitor CQ (1 μm). β-actin was used as the loading control. **E** Quantification of βv integrin expression in **D**, $n = 3$ replicates. Error bars represent SEM (ANOVA; $^{*}p < 0.05$; $^{**}p < 0.01$; ns no significant difference). **F** Internalized biotinylated βv integrin subunit measured using capture ELISA. The wild-type and $wun2^{KD}$ S2 cells were surface-labeled with Sulfo-NHS-LC-biotin, the recycling pathways were inhibited with 0.6 μM PMQ, and surface receptors were allowed to internalize for the indicated times. The internalized biotinylated βv integrin subunit was determined by capture ELISA using βv integrin antibodies and detected by a chromogenic reaction with OPD, and the plates were read at 490 nm. The experimental replicates were compared using the ratio between $wun2^{KD}$ and S2 cells. All experiments were independently repeated thrice. **G** Capture ELISA-based recycling assay of surface-biotinylated βv integrin subunit. Cells were surface-labeled with Sulfo-NHS-LC-biotin and allowed to internalize. Then, cells were cultured in fresh medium for the indicated times to allow receptors recycling to plasma membrane and the recycled receptors were removed. Cells were lysed, and the biotinylated βv integrin subunit internalized in cells was determined by capture ELISA. The proportion of integrin recycled to the cell surface is expressed as the percentage of the pool of integrins labeled during the internalization period. Data are the mean ± SEM of three independent experiments. **H** Macrophages were isolated from $w^{1118}$ and $wun2^{KO}$ prepupae, labeled with anti-βv integrin antibody and allowed to internalize (treated with 1 μM CQ and 0.6 μM PMQ). The distribution of βv integrin in macrophages was observed after staining. Images were background-subtracted and thresholded, $wun2^{KO}$ cells show a reduced number of βv integrin puncta. Scale bar: 10 μm. **I** Quantification of the number of particles in H, (Student's *t* test; $^{****}p < 0.0001$, ten cells were randomly selected for analysis).

Jackson ImmunoResearch Laboratories). Enhanced chemiluminescence western blotting detection was performed according to the supplier's protocol (Pierce). All experiments were repeated at least three times.

### Immunoprecipitations and LC-MS/MS analysis

S2 cells were transfected with full-length *wun2* expression plasmids, harvested, and lysed in 50 mM Tris HCl (pH 7.4), 150 mM NaCl, 1 mM EDTA, and 1% NP40 with complete EDTA-free protease inhibitor. Lysates were centrifuged at 10,000 × *g* for 30 min, and the supernatants were incubated with anti-Flag M2 Affinity Gel (Sigma #A2220) for 6 h at 4 °C. The resin was centrifuged at 1400 × *g* for 1 min and washed thrice with Tris-buffered saline; 50 μL of 2× sodium dodecyl sulfate–polyacrylamide gel electrophoresis (SDS-PAGE) sample buffer was added and boiled for 5 min. Supernatants were subsequently transferred for silver staining or LC-MS/MS analysis (Hoogen Biotech Co.).

### Yeast two-hybrid assays

For binary yeast two-hybrid assays, transmembrane proteins using the split-ubiquitin system, which inserts genes of interest into Cub or Nub as vectors and transforms vectors into yeast THY.AP4 [69]. Yeast was obtained from a stock plate, added to 15 mL yeast peptone dextrose adenine (YPDA) medium, inoculated in a 50 mL sterile tube, and incubated in a shaker overnight at 280 rpm and 30 °C. Next, 300 mL of YPDA was inoculated with 15 mL of overnight culture in autoclaved flasks and incubated with shaking at 280 rpm and 30 °C for 3–4 h. Then, cells were harvested and washed with sterile water, resuspended in 1.8 mL of 0.1 M LiAc, transferred to a 2 mL Eppendorf tube, and centrifuged at 2000 × *g* and 4 °C for 30 s. The supernatant was discarded, and an appropriate amount of 0.1 M LiAc was added to the tube, which was incubated at 25 °C for 30 min. Sterilized PCR tubes were prepared with 10 μL of single-stranded DNA and 1 μg of plasmid DNA for each transformation mix, 70 μL of polyethylene glycol solution, 10 μL of 1 M LiAc, and 20 μL of competent yeast for each transformation. The mixture was stirred and incubated at 30 °C for 30 min, and cells were heat-shocked at 42 °C for 40 min. The yeast was then centrifuged at 2000 × *g* for 1 min, washed with 100 μL of sterile water, resuspended in 50 μL of sterile water, plated on synthetic-defined (SD)-Leu/Trp drop-out plates, and grown for 3–4 days at 30 °C. Finally, three representative colonies were selected and diluted for spot testing. The same concentration of yeast was spotted on selected SD-Ade/His/Trp/Leu plates.

### Embryo immunostaining

Immunostaining was performed according to the method described in previous studies [70, 71]. Briefly, staged embryos were fixed in 4% paraformaldehyde and stained with Crq antibody, which specifically labels macrophages while Dcp-1 antibody labels ACs [70, 72]. Rabbit or mouse fluorescein-coupled secondary antibodies were used at a 1:1000 dilution. Stained embryos were mounted in Vectashield medium, observed using a confocal microscope (C2, Nikon Instruments), and photographed at 20× and 100× magnifications. Images were processed using Adobe Photoshop CS6 and ImageJ.

### Phagocytosis ratio and phagocytic index

The phagocytosis ratio was quantified as the number of engulfed ACs compared to total ACs, and phagocytic index (average number of ACs per hemocyte, PI) was determined as previously described [71]. Phagocytosis ratio and PI were calculated from confocal images acquired from ten embryos in which three confocal image stacks (head, CNS and tail) of 6 sections through macrophages per embryo were taken.

### Cell immunofluorescence assay

S2 or HeLa cells were plated on a cover glass and fixed in 4% paraformaldehyde for 5 min, incubated in 1% bovine serum albumin (BSA) in 0.1% PBS-Tween for 1 h, and then incubated with the antibody overnight at 4 °C in PBS containing 1% BSA and 0.1% Tween. Alexa Fluor 594-conjugated goat anti-rabbit antibody was used at a 1:500 dilution for 1 h. Hoechst 33342 was used to stain cell nuclei. The samples were imaged using a laser scanning confocal microscope (C2, Nikon Instruments).

### Macrophage isolation and immunostaining

Isolation of macrophages from *D. melanogaster* pupae was performed as previously described [73, 74]. Briefly, late third instar larvae were cultured for an additional 1–2 h until the formation of white pupae; ten white pupae were then bled at the dorsal side into a cell culture medium. The cell suspension was transferred to a plate on top of a glass coverslip, and allowed to spread on coverslips for 1 h at 25 °C. For the endocytic trafficking of βv integrin subunits from the cell surface by surface labeling [38, 39], cells were washed with cold PBS and incubated with an anti-HA antibody (1:100) for 30 min on ice. The surface-bound antibody was allowed to internalize for 2 h at 25 °C in SFM medium with 1 μm lysosome inhibitor CQ and 0.6 μm PMQ. Thereafter, the samples were washed with cold PBS, and the remaining antibody at the cell surface was removed through two acid washes (0.2 M acetic acid, 0.5 M NaCl, both in PBS) for 2 min on ice. Subsequently, the cells were fixed, permeabilized, and stained, as described in the cell immunofluorescence assay.

### Phosphate release assay

The malachite green phosphate assay kit (Sigma #MAK307) was used to analyze the enzymatic reaction [75, 76]. The assays were performed in 96-well plates at 25 °C. Briefly, 50 μL of the anti-Flag resin containing the immunocaptured proteins was added to each well, and the phospholipids LPA and C1P were dissolved in 50% and 100% ethanol, respectively, at a final concentration of 500 μM. PA in 100% ethanol was used at a final concentration of 70 μM; S1P was dissolved in methanol to a final concentration of 100 μM and supplemented with protein lysis buffer to a final volume of 80 μL. The enzymatic reaction was stopped with 20 μL of malachite green reagent at the indicated time point and the resulting absorbance was measured at 620 nm on a plate reader (BioTek ELX808) at

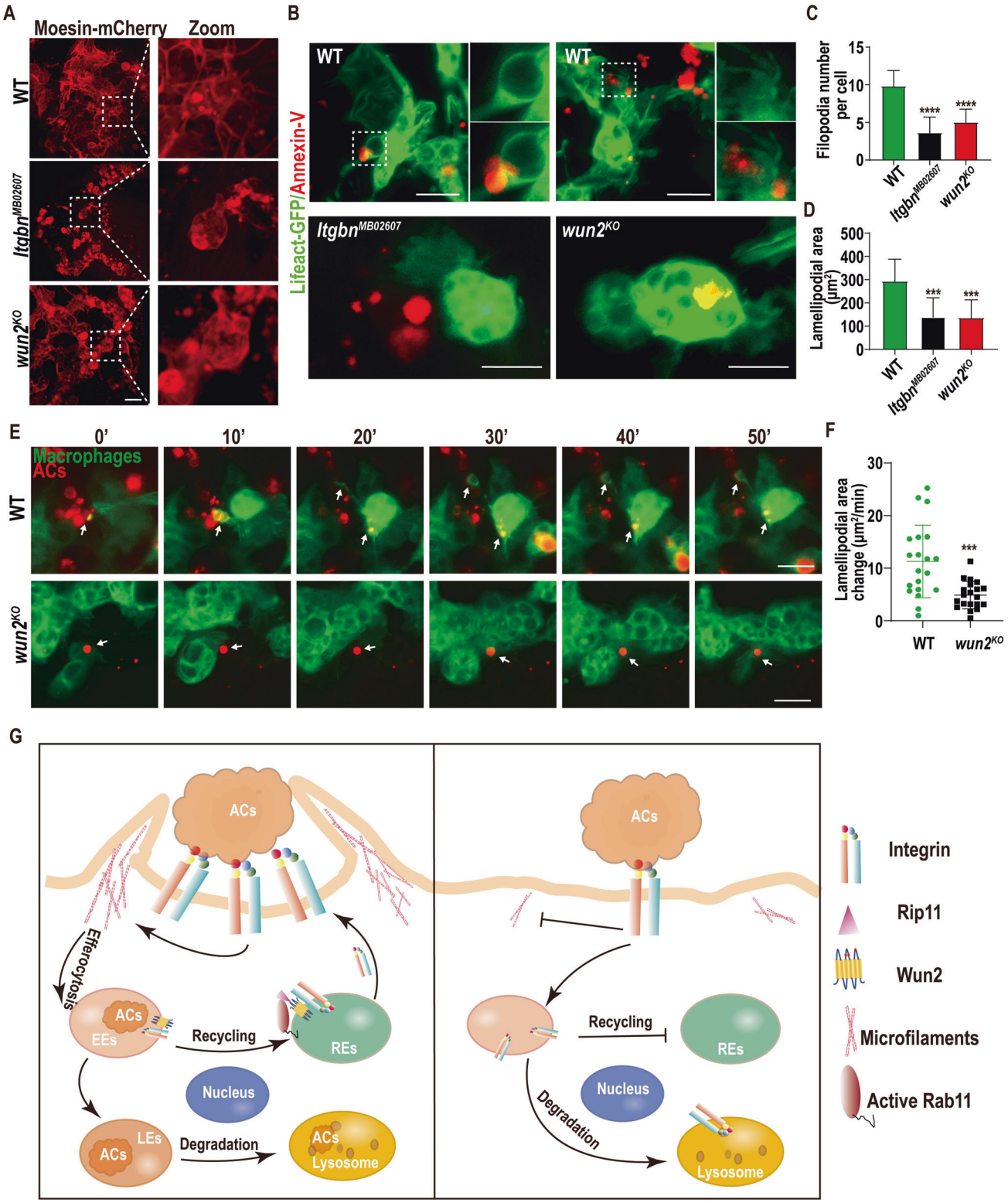


a final volume of 100 µL. Each reaction was performed in triplicate and repeated thrice.

### Integrin internalization

The internalization of integrins was determined by biotinylation [38, 39]. The following steps were performed on ice unless otherwise noted. S2 cells were serum-starved for 1 h, washed twice in cold PBS, labeled with 200 µg/mL Sulfo-NHS-LC-biotin (Thermo Fisher Scientific #A39257) for 30 min at 4 °C, and then incubated in regular growth medium at 25 °C in the presence of 0.6 µM PMQ (recycling pathway inhibitor) for 0, 5, 10, and 15 min to allow internalization. At the indicated times, cells were rapidly transferred to ice, and the medium was aspirated. The cells were washed twice with ice-cold PBS and incubated with 20 mM MesNa (in 50 mM Tris pH 8.6 and 100 mM NaCl) for 15 min to remove surface biotin, and 20 mM iodoacetamide (IAA) was added for 5 min to quench MesNa. Cells were

**Fig. 8 Wun2 is important for F-actin arrangement at the protrusions to envelop ACs. A** Imaging of dispersing macrophages (stage 13) expressing moesin-mCherry (F-actin, red) in wild-type, *Itgbn*$^{MB02607}$, and *wun2*$^{KO}$ embryo. The dashed box is magnified in subsequent panels. Scale bars: 20 μm. **B** Wild-type, *Itgbn*$^{MB02607}$, and *wun2*$^{KO}$ macrophages expressing LifeAct-GFP (F-actin, green) engulfing Annexin-V labeled ACs (red) in stage 13 embryos. The dashed box is magnified in right panels, highlighting F-actin-rich pseudopodia. Scale bars: 10 μm. **C** The number of filopodia per hemocyte in WT 9.8 ± 0.6633, *itgbn* mutant 3.6 ± 0.67 and *wun2* mutant 5 ± 0.5578; **D** The lamellipodial are of WT, *itgbn* mutant and *wun2* mutant, data of **C** and **D** are presented as mean ± SEM ($n = 10$ hemocytes for per phenotypes, ANOVA; ***$p < 0.001$; ****$p < 0.0001$). **E** Time-lapse recordings of ACs clearance in stage 13 embryos. Macrophages are labeled with LifeAct-GFP (green) and ACs are marked with fluorescent Annexin-V (red). Time is in minutes. Scale bars: 10 μm. **F** The average lamellipodial area change per hemocyte in WT and *wun2* mutant (Student's *t* test; ***$p < 0.001$, twenty cells were randomly selected for analysis). **G** Model of the proposed function of Wun2 in endosomal recycling. During efferocytosis, the phagocytic receptor βv integrin subunit triggers downstream signal activation and further promotes the rearrangement of the cytoskeleton polymerization to engulf ACs; βv integrin subunit internalizes with ACs into early endosomes, and Wun2 interacts with βv integrin subunit and Rip11 to facilitate the transfer of the former to recycling endosomes and consequent transport to the plasma membrane. The engulfed ACs are delivered to lysosome for degradation (left). In the absence of Wun2, βv integrin subunit is transferred to lysosomes for degradation, thereby failing to trigger the actin cytoskeleton rearrangement to engulf ACs (right).

lysed (75 mM Tris, 200 mM NaCl, 7.5 mM EDTA, 7.5 mM EGTA, 1.5% Triton X-100, 0.75% IgepalCA-630, and protease inhibitors), and lysates were centrifuged at 20,000 × *g* for 30 min at 4 °C. Supernatants were collected and analyzed using capture enzyme-linked immunosorbent assay (ELISA) or immunoprecipitation. Each reaction was performed in triplicates and repeated thrice.

### Integrin recycling

For the integrin recycling assay, S2 cells were serum-starved for 1 h, washed twice in cold PBS, labeled with 200 μg/mL Sulfo-NHS-LC-biotin (Thermo Fisher Scientific #A39257) for 30 min at 4 °C, and then incubated in regular growth medium (without PMQ) at 25 °C for 30 min to allow integrin internalization. After this period, cells were washed twice with ice-cold PBS and incubated with 20 mM MesNa for 15 min to remove surface biotin; 20 mM iodoacetamide (IAA) was then added for 5 min to quench MesNa. The cells were incubated in regular medium at 25 °C for 0, 5, 10, and 15 min to allow for biotinylated-βv integrin subunit recycling to the plasma membrane. Following a second reduction with MesNa to remove the recycled biotinylated-receptors, IAA was added for 5 min to quench MesNa. Cells were collected and lysed and centrifuged at 20,000 × *g* for 30 min at 4 °C. Supernatants were collected and analyzed using capture ELISA or immunoprecipitation.

### Capture ELISA

Capture ELISA was performed as previously described [38, 39]. Ninety-six-well plates were coated overnight with anti-βv integrin antibodies (diluted at 1:200 in 0.05 M $Na_2CO_3$, pH 9.6) at 4 °C. Unspecific binding was blocked with 5% BSA in PBS-T (0.05% Tween-20 in PBS) for 1 h at 25 °C. Fifty microliters of cell lysate were added for 8 h at 4 °C to capture βv integrin subunit. The cell lysates were then removed and washed with PBS-T twice. Plates were incubated with streptavidin-horseradish peroxidase (HRP) in 1% BSA in PBS-T for 1 h at 4 °C. Biotinylated βv integrin subunit was detected using a chromogenic reaction with o-phenylenediamine (OPD), and the plates were read at 490 nm.

### Proximity labeling with TurboID

Enzyme-catalyzed proximity labeling (PL) is a popular approach for studying the spatial localization and interactions of proteins in living cells. TurboID, the promiscuous ligase, enables nontoxic biotin to label the neighboring proteins [77, 78]. Proteins biotinylated by TurboID were enriched with streptavidin beads and identified by western blotting. Briefly, exponentially grown S2 cells were co-transfected with TurboID-fused construct (bait) and protein vectors (prey); after 36 h, the cells were replaced with fresh culture medium containing 50 μM exogenous biotin for 1 h. The reaction was terminated by cooling cells to 4 °C and washing away excess biotin. Cell pellets were lysed in IP lysis buffer as described above, and centrifuged at 20,000 × *g* for 20 min at 4 °C, and the upper soluble fraction was retained. For enrichment of biotinylated proteins, 20 μL of streptavidin-coated magnetic beads (Thermo Fisher Scientific #88817) were washed twice with the IP lysis buffer and then incubated with lysates containing 2 mg protein for each sample on a rotator for 6 h at 4 °C. For quality control analysis, the beads were washed twice in 50 mM Tris-HCl (pH 7.5) and biotinylated proteins were eluted by boiling the beads in 40 μL of 2× protein loading buffer, run on SDS-PAGE for western blot analysis.

### Live imaging of *D. melanogaster* embryos

Stage 13 embryos were dechorionated in bleach and mounted in Voltalef oil under a coverslip on a gas-permeable culture dish [79, 80]. In brief, embryos were collected from agar plates and washed in the cell strainer using water. Excess water was dried out and the embryos were dechorionated in 50% bleach for 2–3 min. Next, the embryos were extensively rinsed with water until they lost the bleach odor. The embryos were then attached to a coverslip coated with a strip of the heptane glue in the middle. The coverslip was placed in the dehydration chamber for approximately 5 min. After drying, the embryos were covered with halocarbon oil 700 (Sigma, #H8898) to avoid further dehydration. Next, 1 μL of Annexin V (Molecular Probes, #13203) was loaded into a needle, which was attached to a micromanipulator, and all the embryos were sequentially injected with a drop. Images were collected on a confocal microscope (C2; Nikon Instruments). To quantify the duration of ACs clearance, 45-min time-lapse videos were acquired with a z stack taken every 30 s. Time-lapse images were processed using ImageJ.

### Statistical analysis

Statistical analysis was performed using GraphPad Prism software. One-way analysis of variance (ANOVA) or Student's *t* test determined statistical significance at $p < 0.05$. In the plots, error bars represent the standard error of the mean (SEM), "*" stands for $p < 0.05$, "**" for $p < 0.01$, "***" for $p < 0.001$, and "****" for $p < 0.0001$. Ten embryos from each genotype were tested unless indicated otherwise.

## DATA AVAILABILITY

All data are provided in the manuscript and Supplementary files or are available from the corresponding authors upon reasonable request.

## REFERENCES

1. Kumar S, Birge RB. Efferocytosis. Curr Biol. 2016;26:R558–R559.
2. Cheng X, Ferrell JE Jr. Apoptosis propagates through the cytoplasm as trigger waves. Science. 2018;361:607–12.
3. Liu Z, Davidson A. Taming lupus-a new understanding of pathogenesis is leading to clinical advances. Nat Med. 2012;18:871–82.
4. Poon IK, Lucas CD, Rossi AG, Ravichandran KS. Apoptotic cell clearance: basic biology and therapeutic potential. Nat Rev Immunol. 2014;14:166–80.
5. Ley K, Miller YI, Hedrick CC. Monocyte and macrophage dynamics during atherogenesis. Arterioscler Thromb Vasc Biol. 2011;31:1506–16.
6. Mattson MP. Apoptosis in neurodegenerative disorders. Nat Rev Mol Cell Biol. 2000;1:120–9.
7. Wood W, Martin P. Macrophage functions in tissue patterning and disease: New insights from the fly. Dev Cell. 2017;40:221–33.
8. Manaka J, Kuraishi T, Shiratsuchi A, Nakai Y, Higashida H, Henson P, et al. Draper-mediated and phosphatidylserine-independent phagocytosis of apoptotic cells by Drosophila hemocytes/macrophages. J Biol Chem. 2004;279:48466–76.
9. Zhou Z, Hartwieg E, Horvitz HR. CED-1 is a transmembrane receptor that mediates cell corpse engulfment in C. elegans. Cell. 2001;104:43–56.
10. Franc NC, Dimarcq JL, Lagueux M, Hoffmann J, Ezekowitz RA. Croquemort, a novel Drosophila hemocyte/macrophage receptor that recognizes apoptotic cells. Immunity. 1996;4:431–43.

11. Franc NC, Heitzler P, Ezekowitz RA, White K. Requirement for croquemort in phagocytosis of apoptotic cells in Drosophila. Science. 1999;284:1991–4.
12. Nagaosa K, Okada R, Nonaka S, Takeuchi K, Fujita Y, Miyasaka T, et al. Integrin betanu-mediated phagocytosis of apoptotic cells in Drosophila embryos. J Biol Chem. 2011;286:25770–7.
13. Nonaka S, Nagaosa K, Mori T, Shiratsuchi A, Nakanishi Y. Integrin alphaPS3/betanu-mediated phagocytosis of apoptotic cells and bacteria in Drosophila. J Biol Chem. 2013;288:10374–80.
14. Kok BP, Venkatraman G, Capatos D, Brindley DN. Unlike two peas in a pod: lipid phosphate phosphatases and phosphatidate phosphatases. Chem Rev. 2012;112:5121–46.
15. Burnett C, Howard K. Fly and mammalian lipid phosphate phosphatase isoforms differ in activity both in vitro and in vivo. EMBO Rep. 2003;4:793–9.
16. Waggoner DW, Gómez-Muñoz A, Dewald J, Brindley DN. Phosphatidate phosphohydrolase catalyzes the hydrolysis of ceramide 1-phosphate, lysophosphatidate, and sphingosine 1-phosphate. J Biol Chem. 1996;271:16506–9.
17. Hanyu-Nakamura K, Kobayashi S, Nakamura A. Germ cell-autonomous Wunen2 is required for germline development in Drosophila embryos. Development. 2004;131:4545–53.
18. Starz-Gaiano M, Cho NK, Forbes A, Lehmann R. Spatially restricted activity of a Drosophila lipid phosphatase guides migrating germ cells. Development. 2001;128:983–91.
19. Ile KE, Tripathy R, Goldfinger V, Renault AD. Wunen, a Drosophila lipid phosphate phosphatase, is required for septate junction-mediated barrier function. Development. 2012;139:2535–46.
20. Nema R, Kumar A. Sphingosine-1-phosphate catabolizing enzymes predict better prognosis in triple-negative breast cancer patients and correlates with tumor-infiltrating immune cells. Front Mol Biosci. 2021;8:697922.
21. De Franceschi N, Hamidi H, Alanko J, Sahgal P, Ivaska J. Integrin traffic - the update. J Cell Sci. 2015;128:839–52.
22. Sayedyahossein S, Dagnino L. Integrins and small GTPases as modulators of phagocytosis. Int Rev Cell Mol Biol. 2013;302:321–54.
23. Moreno-Layseca P, Icha J, Hamidi H, Ivaska J. Integrin trafficking in cells and tissues. Nat Cell Biol. 2019;21:122–32.
24. Högnäs G, Tuomi S, Veltel S, Mattila E, Murumägi A, Edgren H, et al. Cytokinesis failure due to derailed integrin traffic induces aneuploidy and oncogenic transformation in vitro and in vivo. Oncogene. 2012;31:3597–606.
25. Dozynkiewicz MA, Jamieson NB, Macpherson I, Grindlay J, van den Berghe PV, von Thun A, et al. Rab25 and CLIC3 collaborate to promote integrin recycling from late endosomes/lysosomes and drive cancer progression. Dev Cell. 2012;22:131–45.
26. Muller PA, Caswell PT, Doyle B, Iwanicki MP, Tan EH, Karim S, et al. Mutant p53 drives invasion by promoting integrin recycling. Cell. 2009;139:1327–41.
27. Goto A, Kadowaki T, Kitagawa Y. Drosophila hemolectin gene is expressed in embryonic and larval hemocytes and its knock down causes bleeding defects. Dev Biol. 2003;264:582–91.
28. Stramer B, Moreira S, Millard T, Evans I, Huang CY, Sabet O, et al. Clasp-mediated microtubule bundling regulates persistent motility and contact repulsion in Drosophila macrophages in vivo. J Cell Biol. 2010;189:681–9.
29. Zhang N, Zhang J, Purcell K, Cheng Y, Howard K. The Drosophila protein Wunen repels migrating germ cells. Nature. 1997;385:64–67.
30. Renault AD, Sigal YJ, Morris AJ, Lehmann R. Soma-germ line competition for lipid phosphate uptake regulates germ cell migration and survival. Science. 2004;305:1963–6.
31. Starz-Gaiano M, Cho N, Forbes A, Lehmann R. Spatially restricted activity of a Drosophila lipid phosphatase guides migrating germ cells. Development. 2001;128:983–91.
32. Naslavsky N, Caplan S. The enigmatic endosome - sorting the ins and outs of endocytic trafficking. J Cell Sci. 2018;131:jcs216499.
33. Homma Y, Hiragi S, Fukuda M. Rab family of small GTPases: an updated view on their regulation and functions. FEBS J. 2021;288:36–55.
34. Vetter M, Wang J, Lorentzen E, Deretic D. Novel topography of the Rab11-effector interaction network within a ciliary membrane targeting complex. Small GTPases. 2015;6:165–73.
35. Humtsoe JO, Bowling RA Jr, Feng S, Wary KK. Murine lipid phosphate phosphohydrolase-3 acts as a cell-associated integrin ligand. Biochem Biophys Res Commun. 2005;335:906–19.
36. Humtsoe JO, Feng S, Thakker GD, Yang J, Hong J, Wary KK. Regulation of cell-cell interactions by phosphatidic acid phosphatase 2b/VCIP. EMBO J. 2003;22:1539–54.
37. Shiratsuchi A, Mori T, Sakurai K, Nagaosa K, Sekimizu K, Lee BL, et al. Independent recognition of Staphylococcus aureus by two receptors for phagocytosis in Drosophila. J Biol Chem. 2012;287:21663–72.
38. Bottcher RT, Stremmel C, Meves A, Meyer H, Widmaier M, Tseng HY, et al. Sorting nexin 17 prevents lysosomal degradation of beta1 integrins by binding to the beta1-integrin tail. Nat Cell Biol. 2012;14:584–92.
39. Roberts M, Barry S, Woods A, van der Sluijs P, Norman J. PDGF-regulated rab4-dependent recycling of alphavbeta3 integrin from early endosomes is necessary for cell adhesion and spreading. Curr Biol. 2001;11:1392–402.
40. Raymond MH, Davidson AJ, Shen Y, Tudor DR, Lucas CD, Morioka S, et al. Live cell tracking of macrophage efferocytosis during Drosophila embryo development in vivo. Science. 2022;375:1182–7.
41. Davidson AJ, Wood W. Macrophages use distinct actin regulators to switch engulfment strategies and ensure phagocytic plasticity in vivo. Cell Rep. 2020;31:107692.
42. Rotty JD, Brighton HE, Craig SL, Asokan SB, Cheng N, Ting JP, et al. Arp2/3 complex is required for macrophage integrin functions but is dispensable for FcR phagocytosis and in vivo motility. Dev Cell. 2017;42:498–513.e496.
43. Baumann I, Kolowos W, Voll RE, Manger B, Gaipl U, Neuhuber WL, et al. Impaired uptake of apoptotic cells into tingible body macrophages in germinal centers of patients with systemic lupus erythematosus. Arthritis Rheum. 2002;46:191–201.
44. Heckmann BL, Tummers B, Green DR. Crashing the computer: apoptosis vs. necroptosis in neuroinflammation. Cell Death Differ. 2019;26:41–52.
45. Fricker M, Neher JJ, Zhao JW, Théry C, Tolkovsky AM, Brown GC. MFG-E8 mediates primary phagocytosis of viable neurons during neuroinflammation. J Neurosci. 2012;32:2657–66.
46. Sano H, Renault AD, Lehmann R. Control of lateral migration and germ cell elimination by the Drosophila melanogaster lipid phosphate phosphatases Wunen and Wunen 2. J Cell Biol. 2005;171:675–83.
47. Tattikota SG, Cho B, Liu Y, Hu Y, Barrera V, Steinbaugh MJ, et al. A single-cell survey of Drosophila blood. Elife. 2020;9:e54818.
48. Bréart B, Ramos-Perez WD, Mendoza A, Salous AK, Gobert M, Huang Y, et al. Lipid phosphate phosphatase 3 enables efficient thymic egress. J Exp Med. 2011;208:1267–78.
49. Renault AD, Kunwar PS, Lehmann R. Lipid phosphate phosphatase activity regulates dispersal and bilateral sorting of embryonic germ cells in Drosophila. Development. 2010;137:1815–23.
50. Ren H, Panchatcharam M, Mueller P, Escalante-Alcalde D, Morris AJ, Smyth SS. Lipid phosphate phosphatase (LPP3) and vascular development. Biochim Biophys Acta. 2013;1831:126–32.
51. Gutierrez-Martinez E, Fernandez-Ulibarri I, Lazaro-Dieguez F, Johannes L, Pyne S, Sarri E, et al. Lipid phosphate phosphatase 3 participates in transport carrier formation and protein trafficking in the early secretory pathway. J Cell Sci. 2013;126:2641–55.
52. Ullrich O, Reinsch S, Urbé S, Zerial M, Parton RG. Rab11 regulates recycling through the pericentriolar recycling endosome. J Cell Biol. 1996;135:913–24.
53. Cox D, Lee DJ, Dale BM, Calafat J, Greenberg S. A Rab11-containing rapidly recycling compartment in macrophages that promotes phagocytosis. Proc Natl Acad Sci USA. 2000;97:680–5.
54. Jiang C, Liu Z, Hu R, Bo L, Minshall RD, Malik AB, et al. Inactivation of Rab11a GTPase in macrophages facilitates phagocytosis of apoptotic neutrophils. J Immunol. 2017;198:1660–72.
55. Nader GP, Ezratty EJ, Gundersen GG. FAK, talin and PIPKIγ regulate endocytosed integrin activation to polarize focal adhesion assembly. Nat Cell Biol. 2016;18:491–503.
56. Jonker CTH, Galmes R, Veenendaal T, Ten Brink C, van der Welle REN, Liv N, et al. Vps3 and Vps8 control integrin trafficking from early to recycling endosomes and regulate integrin-dependent functions. Nat Commun. 2018;9:792.
57. Steinberg F, Heesom KJ, Bass MD, Cullen PJ. SNX17 protects integrins from degradation by sorting between lysosomal and recycling pathways. J Cell Biol. 2012;197:219–30.
58. Böttcher RT, Stremmel C, Meves A, Meyer H, Widmaier M, Tseng HY, et al. Sorting nexin 17 prevents lysosomal degradation of β1 integrins by binding to the β1-integrin tail. Nat Cell Biol. 2012;14:584–92.
59. Prekeris R, Klumperman J, Scheller RH. A Rab11/Rip11 protein complex regulates apical membrane trafficking via recycling endosomes. Mol Cell. 2000;6:1437–48.
60. Cho W. Membrane targeting by C1 and C2 domains. J Biol Chem. 2001;276:32407–10.
61. Oancea E, Meyer T. Protein kinase C as a molecular machine for decoding calcium and diacylglycerol signals. Cell. 1998;95:307–18.
62. Gijón MA, Spencer DM, Kaiser AL, Leslie CC. Role of phosphorylation sites and the C2 domain in regulation of cytosolic phospholipase A2. J Cell Biol. 1999;145:1219–32.
63. Lindsay AJ, McCaffrey MW. The C2 domains of the class I Rab11 family of interacting proteins target recycling vesicles to the plasma membrane. J Cell Sci. 2004;117:4365–75.
64. Svitkina TM. Ultrastructure of protrusive actin filament arrays. Curr Opin Cell Biol. 2013;25:574–81.
65. Trapnell C, Pachter L, Salzberg SL. TopHat: discovering splice junctions with RNA-Seq. Bioinformatics. 2009;25:1105–11.
66. Trapnell C, Williams BA, Pertea G, Mortazavi A, Kwan G, van Baren MJ, et al. Transcript assembly and quantification by RNA-Seq reveals unannotated

transcripts and isoform switching during cell differentiation. Nat Biotechnol. 2010;28:511–5.
67. Cuttell L, Vaughan A, Silva E, Escaron CJ, Lavine M, Van Goethem E, et al. Undertaker, a Drosophila Junctophilin, links Draper-mediated phagocytosis and calcium homeostasis. Cell. 2008;135:524–34.
68. Silva EA, Burden J, Franc NC. In vivo and in vitro methods for studying apoptotic cell engulfment in Drosophila. Methods Enzymol. 2008;446:39–59.
69. Obrdlik P, El-Bakkoury M, Hamacher T, Cappellaro C, Vilarino C, Fleischer C, et al. K+ channel interactions detected by a genetic system optimized for systematic studies of membrane protein interactions. Proc Natl Acad Sci USA. 2004;101:12242–7.
70. Shlyakhover E, Shklyar B, Hakim-Mishnaevski K, Levy-Adam F, Kurant E. Drosophila GATA factor serpent establishes phagocytic ability of embryonic macrophages. Front Immunol. 2018;9:266.
71. Silva E, Au-Yeung HW, Van Goethem E, Burden J, Franc NC. Requirement for a Drosophila E3-ubiquitin ligase in phagocytosis of apoptotic cells. Immunity. 2007;27:585–96.
72. Petrignani B, Rommelaere S, Hakim-Mishnaevski K, Masson F, Ramond E, Hilu-Dadia R, et al. A secreted factor NimrodB4 promotes the elimination of apoptotic corpses by phagocytes in Drosophila. EMBO Rep. 2021;22:e52262.
73. Nagel BM, Bechtold M, Rodriguez LG, Bogdan S. Drosophila WASH is required for integrin-mediated cell adhesion, cell motility and lysosomal neutralization. J Cell Sci. 2017;130:344–59.
74. Sander M, Squarr AJ, Risse B, Jiang X, Bogdan S. Drosophila pupal macrophages-a versatile tool for combined ex vivo and in vivo imaging of actin dynamics at high resolution. Eur J Cell Biol. 2013;92:349–54.
75. Takeuchi M, Harigai M, Momohara S, Ball E, Abe J, Furuichi K, et al. Cloning and characterization of DPPL1 and DPPL2, representatives of a novel type of mammalian phosphatidate phosphatase. Gene. 2007;399:174–80.
76. Yang Z, Zhang Y, Shen T, Xie Y, Mao Y, Ji C. Cloning, expression and biochemical characterization of a novel, moderately thermostable GDSL family esterase from Geobacillus thermodenitrificans T2. J Biosci Bioeng. 2013;115:133–7.
77. Zhang B, Zhang Y, Liu JL. Highly effective proximate labeling in Drosophila. G3. 2021;11:jkab077.
78. Branon TC, Bosch JA, Sanchez AD, Udeshi ND, Svinkina T, Carr SA, et al. Efficient proximity labeling in living cells and organisms with TurboID. Nat Biotechnol. 2018;36:880–7.
79. Evans IR, Zanet J, Wood W, Stramer BM. Live imaging of Drosophila melanogaster embryonic hemocyte migrations. J Vis Exp. 2010;36:1696.
80. Shklyar B, Shklover J, Kurant E. Live imaging of apoptotic cell clearance during Drosophila embryogenesis. J Vis Exp. 2013;78:50151.

## ACKNOWLEDGEMENTS

We thank the Bloomington *Drosophila* Stock Center for the *Drosophila melanogaster* strains. Additionally, we thank Editage (www.editage.cn) for English language editing.

## AUTHOR CONTRIBUTIONS

HX and NG conceived the study. NG and QZ performed most of the experiments. XWL, YZW, and ZL provided the materials and performed some experiments. HX, NG, and QZ wrote the manuscript.

## FUNDING

This study was partially supported by the National Natural Science Foundation Key Project (breeding program) of China (Grant no. 91954114 to HX), National Natural Science Foundation of China (Grant no. 31871387 to HX), National Natural Science Foundation of China Youth Program (Grant no. 31801164 to QZ), the program of Innovative Research Team for the Central Universities (Grant no. GK202001004 to HX), and the Fundamental Research Key Project Funds for the Central Universities (Grant no. GK202007009 to HX).

## COMPETING INTERESTS

The authors declare no competing interests.

## ETHICS APPROVAL AND CONSENT TO PARTICIPATE

All animal care and experiments were performed according to the "Guide for the Care and Use of Laboratory Animals," which were approved by the Institutional Animal Care and Use Committee at Shaanxi Normal University, and all manipulations were conducted in accordance with established guidelines.

## ADDITIONAL INFORMATION

**Supplementary information** The online version contains supplementary material available at https://doi.org/10.1038/s41418-022-01039-3.

**Correspondence** and requests for materials should be addressed to Hui Xiao.

**Reprints and permission information** is available at http://www.nature.com/reprints

**Publisher's note** Springer Nature remains neutral with regard to jurisdictional claims in published maps and institutional affiliations.